



Primary structure materials – Test results (first batch)

J. Berthe, A. Deudon, C. Huchette, G. Roger, G. Leplat, G. Portemont

Future Sky Safety is a Joint Research Programme (JRP) on Safety, initiated by EREA, the association of European Research Establishments in Aeronautics. The Programme contains two streams of activities: 1) coordination of the safety research programmes of the EREA institutes and 2) collaborative research projects on European safety priorities.

This deliverable is produced by the Project P7 “Mitigating Risks of Fire, Smoke and Fumes”, and belongs to the first work package, the aim of which is to improve characterization capabilities and understanding with respect to the fire and high temperature behaviour of primary structure CFRP materials. Test results from a first batch of T700/M21 test specimens are presented in this report.

Programme Manager	Michel Piers, NLR
Operations Manager	Lennaert Speijker, NLR
Project Manager (P7)	Eric Deletombe, ONERA

Grant Agreement No.	640597
Document Identification	D7.4
Status	Approved
Version	2.1
Classification	Public

Project: Mitigating risks of fire, smoke and fumes
Reference ID: FSS_P7_ONERA_D7.4
Classification: Public



This page is intentionally left blank

Contributing partners

Company	Name
ONERA	J. Berthe, A. Deudon, G. Portemont
ONERA	G. Leplat
ONERA	C. Huchette, G Roger

Document Change Log

Version	Issue Date	Remarks
1.0	21-07-2016	First formal release
2.0	28-06-2016	Second formal release
2.1	19-06-2019	Dissemination level changed from Confidential to Public

Approval status

Prepared by: (name)	Company	Role	Date
Gillian Leplat	ONERA	Main Author	06-07-2016
Checked by: (name)	Company	Role	Date
Julien Berthe	ONERA	Quality assurance	21-07-2016
Approved by: (name)	Company	Role	Date
Eric Deletombe	ONERA	Project Manager (P7)	21-07-2016
Lennaert Speijker	NLR	Operations Manager	26-08-2016

Acronyms

Acronym	Definition
A/C	Aircraft (Commercial)
ASTM	American Society for Testing and Materials
CFRP	Carbon Fibre Reinforced Plastics
DSC	Differential Scanning Calorimetry
FSS	Future Sky Safety
JRI	Joint Research Initiative
P7	FSS Project n°7
PCRD	Programme-cadre de recherche et de développement:
TGA	Thermo Gravimetric Analysis
WP	Workpackage

EXECUTIVE SUMMARY

Problem Area

An objective of the Project P7 “Mitigating the risk of fire, smoke and fumes” of Future Sky Safety (FSS) is to support increasing safety - meaning here reduce the number of fatalities - with respect to fire related issues (in-flight or post-crash). First, many studies on the current flights show that about 50% of the fatalities in case of aircraft accidents are linked to situations where fire is involved. Hundreds of fatalities could be saved per year if fire effects on the primary structure or in the cabin environment were mitigated. Second, the development of larger, more electric and more lightweight aircraft (with an increase use of Carbon Fibre Reinforced Plastics (CFRP) composite parts in aircraft design, such as fuselage panels, engine carters, engine exhausts, etc) raises several safety questions with respect to unknown behaviours of the materials and structures when exposed to fire. But the scope of this problem is large, embracing a variety of problems and solutions: the use of fireproof and less toxic materials, the early detection of fire, the simulation of passengers’ evacuation, etc. In the FSS research programme, it was decided to address the fire issue as part of Theme 4: “Building the Ultra-resilient Vehicles”. It means that the research work is focused on material and structural questions, and aims at mitigating fire related safety risks when/by introducing new generation of materials in future aircraft design (incl. possible eco-friendly ones). Considering this focus, it must be noticed that very few test results are available today to the research community, because of obvious costs (test facilities, destructive tests, specimens and sensors) and industry confidentiality reasons. A large part of the project P7 – to which this deliverable relates - is dedicated to develop and share experimental testing facilities and test results, with a clear partnership added value between EU Research Establishments, Academia and Industry being reached.

For new aircraft concepts, the application of CFRP is considered in the primary structure of the wing and the fuselage. Such airplane exhibits novel or unusual design features leading to a gap with the technology envisioned in the airworthiness standards dedicated to transport category airplanes. A specific concern is for safety issue pertaining to aircraft passengers with respect to crashworthiness and to fire behaviour of composite materials. Enhancing the understanding of aircraft fire performance guarantees aircraft occupants a significant safety increase to come out unharmed in case of fire incident or in crash situation. More particularly, occupant safety improvements with regard to evacuation when engine kerosene fire is developing outside will be linked to an enhancement of knowledge about the carbon epoxy materials behaviour and degradation under severe temperature conditions and fire exposure. In terms of fumes toxicity, self-extinguishability and heat generation, the use of carbon epoxy composite materials for primary structures not only brings specific questions regarding the passengers safety, but also regarding the rescue team efficiency and safety. In terms of structures design, it is crucial to accurately understand and compare the safe, damaged (impact, crash) and decomposed (fire) materials performances, in terms of mechanical strength (load carrying) and fireproofness.

Description of Work

The objective of FSS P7 work package WP7.1 “Understanding and characterising the fire behaviour of primary structure composite materials (epoxy resins, standard CFRP)” is to enhance knowledge concerning the fire behaviour and performance of CFRP primary structure composite materials, in order to better predict safety and survivability issues in case of fire incident or post-crash situation. Such predictions rely on physical models and numerical tools which need to be developed based on exhaustive material (characterisation) and components (validation) experimental testing. The objective of WP7.1 is to produce a comprehensive experimental database for a reference material to be shared by the European research community as a basis for material model development of the fire behaviour and degradation of CFRP materials. The T700GC/M21 material has been proposed to be used in this WP7.1 because a lot of published results already exist about its standard mechanical behaviour which the project can build on. For this purpose, existing testing protocols have to be adapted, improved or invented. FSS P7 deliverable D7.1 “Plan of Experiments – Primary Structures Materials – Final Requirements, Selection and Specification of Materials and Tests” [1] included a list of complementary tests which could be developed and performed to complete an already existing database with respect to:

- Mechanical and thermo-mechanical properties of virgin and charred material,
- Dynamic degradation phenomena (incl. ignition of combustible gases inside the CFRP laminate) during the fire exposure time,
- Fire resistance of damaged composite panels to direct exposure to flame impact.

This report presents the test results from a first batch of T700/M21 test specimens.

Results & Conclusions

In the last past years, ONERA has developed a test facility to provide thermophysical properties characterisation of anisotropic materials. Especially, it can assess simultaneously the specific heat and the 3 main components of the thermal conductivity tensor as a function of temperature. It is based on thermographic measurements of the material thermal response subjected to a pure radiative laser heating. The test facility was carried out on the selected T700GC/M21 CFRP material studied in 2 stacking sequences to the identified properties at the virgin state (i.e. below glass transition and pyrolysis).

In precedent studies, the thermal degradation of epoxy matrix reinforced by carbon fibre composite materials has been performed at Onera. During these studies, three main chemical reactions have been identified: pyrolysis of the matrix, oxidation of the char produced by the pyrolysis of the matrix and oxidation of the fibres. To succeed in, Thermo Gravimetric Analysis (TGA) and Differential Scanning Calorimetry (DSC) experiments have been carried out in order to identify a thermal degradation model adapted to composite material. In this deliverable, only the first TGA results for the material manufactured and provided by CEiiA are presented. A discussion on the characterisation of the “volume” oxidation versus “surface” oxidation is also proposed.

Concerning the mechanical properties of T700GC/M21 CFRP material, original mechanical tests have been defined and performed on an electromechanical testing device equipped with an environmental chamber. The experimental setups have been adapted from ASTM standard procedures in order to be used at elevated temperatures. The preliminary results of these tests which are presented in the present document: they led to the selection and specification of a dedicated test protocol. It will be applied on several T700GC/M21 stacking sequences for different displacement speeds and different environmental temperatures.

Applicability

The obtained test results are complementary to existing ones on T700GC/M21 which are available in the open literature. Once published in journal papers they will permit code developers (academic) and users (industry) to:

- get input data for numerical simulations,
- address the question of the validity of the state-of-the-art models they use (capability to reproduce the observed phenomena),
- propose future developments where lacks are identified.

In the end the composite structures design capabilities could be improved either through increase of confidence in the existing tools, or thanks to new developments based on the gained knowledge.

Project: Mitigating risks of fire, smoke and fumes
Reference ID: FSS_P7_ONERA_D7.4
Classification: Public



This page is intentionally left blank

TABLE OF CONTENTS

Contributing partners	3
Document Change Log	3
Approval status	3
Acronyms	4
Executive Summary	5
List of Figures	11
List of Tables	13
1 Introduction	14
1.1. The Programme	14
1.2. Project context	14
1.3. Research objectives	16
1.4. Approach	16
1.5. Structure of the document	17
2 Material	19
3 Thermal conductivity tensor and heat capacity	20
3.1. Experimental method	20
3.1.1. BLADE facility description	20
3.1.2. Measurement technique	21
3.1.3. Inverse heat conduction method for the laser source characterisation	22
3.1.4. Global thermophysical properties assessment of homogenised orthotropic composite materials	25
3.2. Results overview and global properties analysis	26
3.2.1. Preparation of the test coupons	26
3.2.2. Test matrix	28
3.2.3. Test protocol	29
3.2.4. Optimisation process	29
3.2.5. Thermophysical properties of the unidirectional composite laminate	30
3.2.6. Thermophysical properties of the quasi-isotropic composite laminate	42
4 Thermochemical properties	54
4.1. Thermogravimetric analysis	54
4.1.1. Neutral atmosphere: Nitrogen ambiance	54
4.1.2. Oxidation atmosphere: Air ambiance	55
4.2. Discussion and further works	58

5	Thermo-Mechanical properties	60
5.1.	In-plane compression	60
5.2.	Dynamic Mechanical Analysis	63
5.2.1.	DMA experiments on unidirectional laminate	63
5.2.2.	Results and further works	65
6	Conclusions and recommendations	66
6.1.	Conclusions	66
6.2.	Recommendations	66
7	References	68

LIST OF FIGURES

FIGURE 1 - ILLUSTRATION OF THE BLADE FACILITY: SETUP AND INSTRUMENTATION	20
FIGURE 2 - PRINCIPLE OF THE EXPERIMENTS: THERMO-PHYSICAL CHARACTERISATION AND LASER-INDUCED DECOMPOSITION OF CHARRING MATERIALS	21
FIGURE 3 - RESULTS OF THE INVERSE HEAT CONDUCTION METHOD FOR TEST #003 AT $t = 5 s$	24
FIGURE 4 - INVERSE METHOD PRINCIPLE FOR THERMOPHYSICAL PROPERTIES ASSESSMENT.....	26
FIGURE 5 - ITERATIVE ALGORITHM OF THE INVERSE METHOD FOR THERMOPHYSICAL PROPERTIES ASSESSMENT	26
FIGURE 6 - WATER JET CUT TEST COUPONS	27
FIGURE 7 - RESULTS COMPARISON FOR THE OPTIMISATION RUN #1 ON THE TEMPERATURE RANGE [22 – 40 °C] FOR T700GC-M21-UD8.....	31
FIGURE 8 - RESULTS COMPARISON FOR THE OPTIMISATION RUN #2 ON THE TEMPERATURE RANGE [22 – 60 °C]	32
FIGURE 9 - RESULTS COMPARISON FOR THE OPTIMISATION RUN #3 ON THE TEMPERATURE RANGE [40 – 60 °C]	33
FIGURE 10 - RESULTS COMPARISON FOR THE OPTIMISATION RUN #4 ON THE TEMPERATURE RANGE [40 – 80 °C]	34
FIGURE 11 - RESULTS COMPARISON FOR THE OPTIMISATION RUN #5 ON THE TEMPERATURE RANGE [60 – 80 °C]	35
FIGURE 12 - COMPARISON OF THE SPECIFIC HEAT IDENTIFICATIONS ON THE DIFFERENT TEMPERATURE RANGES FOR THE T700GC-M21-UD8 COMPOSITE LAMINATE	36
FIGURE 13 - COMPARISON OF THE THERMAL CONDUCTIVITY k_{xx} IDENTIFICATIONS ON THE DIFFERENT TEMPERATURE RANGES FOR THE T700GC-M21-UD8 COMPOSITE LAMINATE	36
FIGURE 14 - COMPARISON OF THE THERMAL CONDUCTIVITY k_{yy} IDENTIFICATIONS ON THE DIFFERENT TEMPERATURE RANGES FOR THE T700GC-M21-UD8 COMPOSITE LAMINATE	37
FIGURE 15 - COMPARISON OF THE THERMAL CONDUCTIVITY k_{zz} IDENTIFICATIONS ON THE DIFFERENT TEMPERATURE RANGES FOR THE T700GC-M21-UD8 COMPOSITE LAMINATE	37
FIGURE 16 - IDENTIFICATION OF THE SPECIFIC HEAT ON THE WHOLE TEMPERATURE RANGE FOR THE T700GC-M21-UD8 COMPOSITE LAMINATE	39
FIGURE 17 - IDENTIFICATION OF THE THERMAL CONDUCTIVITY k_{xx} ON THE WHOLE TEMPERATURE RANGE FOR THE T700GC-M21-UD8 COMPOSITE LAMINATE	39
FIGURE 18 - IDENTIFICATION OF THE THERMAL CONDUCTIVITY k_{yy} ON THE WHOLE TEMPERATURE RANGE FOR THE T700GC-M21-UD8 COMPOSITE LAMINATE	40
FIGURE 19 - IDENTIFICATION OF THE THERMAL CONDUCTIVITY k_{zz} ON THE WHOLE TEMPERATURE RANGE FOR THE T700GC-M21-UD8 COMPOSITE LAMINATE	40
FIGURE 20 - k_{zz} PROPERTY EVOLUTION AT HIGHER TEMPERATURES FOR THE T700GC-M21-UD8 COMPOSITE LAMINATE....	41
FIGURE 21 - RESULTS COMPARISON FOR THE OPTIMISATION RUN #6 ON THE TEMPERATURE RANGE [22 – 40 °C]	43
FIGURE 22 - RESULTS COMPARISON FOR THE OPTIMISATION RUN #7 ON THE TEMPERATURE RANGE [22 – 60 °C]	44
FIGURE 23 - RESULTS COMPARISON FOR THE OPTIMISATION RUN #8 ON THE TEMPERATURE RANGE [40 – 60 °C]	45
FIGURE 24 - RESULTS COMPARISON FOR THE OPTIMISATION RUN #9 ON THE TEMPERATURE RANGE [40 – 80 °C]	46
FIGURE 25 - RESULTS COMPARISON FOR THE OPTIMISATION RUN #10 ON THE TEMPERATURE RANGE [60 – 80 °C]	47
FIGURE 26 - COMPARISON OF THE SPECIFIC HEAT IDENTIFICATIONS ON THE DIFFERENT TEMPERATURE RANGES FOR THE T700GC-M21-QI8 COMPOSITE LAMINATE	49

FIGURE 27 - COMPARISON OF THE THERMAL CONDUCTIVITY k_{xx} IDENTIFICATIONS ON THE DIFFERENT TEMPERATURE RANGES FOR THE T700GC-M21-Q18 COMPOSITE LAMINATE49

FIGURE 28 - COMPARISON OF THE THERMAL CONDUCTIVITY k_{yy} IDENTIFICATIONS ON THE DIFFERENT TEMPERATURE RANGES FOR THE T700GC-M21-Q18 COMPOSITE LAMINATE50

FIGURE 29 - COMPARISON OF THE THERMAL CONDUCTIVITY k_{zz} IDENTIFICATIONS ON THE DIFFERENT TEMPERATURE RANGES FOR THE T700GC-M21-Q18 COMPOSITE LAMINATE50

FIGURE 30 - IDENTIFICATION OF THE SPECIFIC HEAT ON THE WHOLE TEMPERATURE RANGE FOR THE T700GC-M21-Q18 COMPOSITE LAMINATE51

FIGURE 31 - IDENTIFICATION OF THE THERMAL CONDUCTIVITY k_{xx} ON THE WHOLE TEMPERATURE RANGE FOR THE T700GC-M21-Q18 COMPOSITE LAMINATE.....52

FIGURE 32 - IDENTIFICATION OF THE THERMAL CONDUCTIVITY k_{yy} ON THE WHOLE TEMPERATURE RANGE FOR THE T700GC-M21-Q18 COMPOSITE LAMINATE.....52

FIGURE 33 - IDENTIFICATION OF THE THERMAL CONDUCTIVITY k_{zz} ON THE WHOLE TEMPERATURE RANGE FOR THE T700GC-M21-Q18 COMPOSITE LAMINATE.....53

FIGURE 34 - MASS LOSS WITH TEMPERATURE UNDER NITROGEN ATMOSPHERE AT DIFFERENT RAMP TEMPERATURES55

FIGURE 35 - MASS LOSS WITH TEMPERATURE UNDER AIR AT DIFFERENT RAMP TEMPERATURES56

FIGURE 36 - MASS LOSS WITH TEMPERATURE UNDER AIR AT DIFFERENT RAMP TEMPERATURES56

FIGURE 37 - MASS LOSS VERSUS TIME UNDER AIR AT DIFFERENT RAMP TEMPERATURES.....57

FIGURE 38 – STRESS-STRAIN CURVES OBTAINED FOR COMPRESSIVE TESTS ON T700GC/M21 [0]₁₆ LAMINATES WITH TWO DIFFERENT EXPERIMENTAL SETUPS: ASTM D3410 (IN RED) AND ONERA MIXED LOADING (IN BLUE)61

FIGURE 39 – STRESS-STRAIN CURVES OBTAINED FOR COMPRESSIVE TESTS ON T700GC/M21 [0]₁₆ LAMINATES WITH GAUGES GLUED ON BOTH SIDES OF THE SPECIMEN.....62

FIGURE 40 -DMA ON AN UD90 SAMPLE, LOSS FACTOR WITH TEMPERATURE63

FIGURE 41 -DMA ON AN UD90 SAMPLE, ELASTIC MODULUS (GPA) WITH TEMPERATURE64

LIST OF TABLES

TABLE 1 - PROPERTIES OF THE PURE TITANIUM REFERENCE COUPON.....	22
TABLE 2 - TEST MATRIX FOR THE LASER SOURCE CHARACTERISATION.....	23
TABLE 3 – COMPARISON OF MAXIMUM HEAT FLUX DENSITIES AND INTEGRATED POWERS.....	24
TABLE 4 - REFERENCE OF THE TEST COUPONS	27
TABLE 5 - TEST MATRIX FOR THE THERMOPHYSICAL PROPERTIES ASSESSMENT	28
TABLE 6 - TESTS USED FOR THE IDENTIFICATION OF THE THERMOPHYSICAL PROPERTIES OF THE T700GC-M21-UD8 COMPOSITE LAMINATE.....	30
TABLE 7 - COMPUTATIONAL MATRIX FOR THE IDENTIFICATION OF THE THERMOPHYSICAL PROPERTIES OF THE T700GC-M21-UD8 COMPOSITE LAMINATE.....	30
TABLE 8 - TESTS USED FOR THE IDENTIFICATION OF THE THERMOPHYSICAL PROPERTIES OF THE T700GC-M21-Q18 COMPOSITE LAMINATE.....	42
TABLE 9 - COMPUTATIONAL MATRIX FOR THE IDENTIFICATION OF THE THERMOPHYSICAL PROPERTIES OF THE T700GC-M21-Q18 COMPOSITE LAMINATE.....	42
TABLE 10 - COMPARISON OF THE MAXIMUM STRESS OBTAINED WITH GLASS/EPOXY TABS, ALUMINUM TABS AND WITHOUT TABS	61

1 INTRODUCTION

1.1. The Programme

Horizon 2020 is the biggest EU Research and Innovation platform ever with nearly €80 billion of funding available over 7 years (2014 to 2020) – in addition to the private investment that this money will attract. Within this frame, EREA, the association of European Research Establishments in Aeronautics has proposed Future Sky program: a Joint Research Initiative in which development and integration of aviation technologies is taken to the European level. Future Sky is based on the alignment of national institutional research for aviation by setting up joint research programs: the first one to be launched in 2015 was the Future Sky Safety programme (<http://www.futuresky.eu/projects/safety>), because safety is a transverse domain of common interest to all stakeholders and with reduced competitive aspects. Four themes and seven projects (5 have already started) were identified (Runway Excursions, Total System Risk Assessment, Human Performance Envelope, Organizational Accidents, and Fire Smoke and Fumes). The work presented in this document belongs to the P7 project “Mitigating Risks of Fire, Smoke and Fumes”.

1.2. Project context

The reason of the “Mitigating Risks of Fire, Smoke and Fumes” project proposal came from the development of larger, more electric and more lightweight aircraft (with an increase use of CFRP composite parts in A/C design, such as fuselage panels, wings, engine carters, engine exhausts, etc). Such airplane exhibits novel or unusual design features leading to a gap with the technology envisioned in the airworthiness standards dedicated to transport category airplanes, which also raises several safety questions with respect to unknown behaviors of the materials and structures. A specific concern is for safety issue pertaining to aircraft passengers with respect to crashworthiness and to fire behavior of composite aircraft structures. But the scope of this problem is large, embracing a variety of problems and solutions: the use of fireproof and less toxic materials, the early detection of fire, the simulation of passengers’ evacuation, etc. And few researches have been funded yet by the EU commission on this subject. It was decided to address the fire issue in the FSS research program as part of Theme 4: “Building the Ultra-resilient Vehicles”. It means that the research work focuses on material and structural questions, and aims at mitigating fire related safety risks when/by introducing new generation of materials in future aircraft design (incl. possible eco-friendly ones).

Enhancing the understanding of aircraft fire performance guarantees aircraft occupants a significant safety increase to come out unharmed in case of fire incident or in crash situation. More particularly, occupant safety improvements with regard to evacuation when engine kerosene fire is developing outside will be linked to an enhancement of knowledge about the carbon epoxy materials behavior and degradation under severe temperature conditions and fire exposure. In terms of fumes toxicity, self-extinguishability, heat generation and degradation products under elevated temperature or fire exposure, the use of composite materials in cabin environment also brings specific questions regarding passengers

and crew safety. Beside of this some concerns also exist about the impact of various innovations on on-board air quality. Multiple investigations have been carried out on hypothetical air contamination by oil ingredients and on the potential impact of such contamination on occupants' health, both in short term and in long term. The more general question of any possible kinds of impact on on-board air quality then raised, that can be due for instance to the introduction of new materials in the design that could react with more and more electrical heating or new engine systems.

The objectives of the EU in terms of increasing air transport safety are reminded in the annual EASA Safety Plan. In this perspective, the P7 objective is to contribute to the reduction of the number of air transport fatalities with respect to fire related issues (in-flight or post-crash). Indeed many studies show that about 50% of the fatalities in case of aircraft accidents are linked to situations where fire is involved. Many fatalities could be saved per year if fire effects on the primary structure or in the cabin environment were mitigated.

In this context, the mechanical behavior and decomposition of organic matrix and carbon fibres of composite materials at elevated temperature or under fire exposure have to be better known, for safety reasons and also health (onboard air quality) issues. Improved material solutions (for primary structures or cabin environment) should also be proposed when needed.

The P7 project "Mitigate risks of fire, smoke and fumes" [2] addresses on the one hand effects of fire on materials (production of heat, toxic fumes and smokes), and on the other hand effects of fire on structures (burnthrough, strength) that can endanger the passengers' life directly (exposure) or indirectly (evacuation). The scope of the works covers both primary structures materials (e.g. epoxy resin, carbon fiber reinforced polymers) and cabin materials (e.g. phenolic polymers, glass fiber reinforced plastics). The P7 project has been split into three work packages according to the expected impacts that were claimed for this 3 years research work:

- WP7.1: the first work package aims at improving the knowledge about effects of fire on materials and structures. It would mainly concern standard epoxy resins and carbon fibers reinforced polymer materials (primary structures),
- WP7.2: the second work package aims at proposing improved materials solutions, mainly to mitigate fire, smoke and fumes. It would concern new materials (primary structures and cabin), the properties of which will be compared to standard ones,
- WP7.3: the third work package aims at analyzing possible effects on the on-board air quality that the introduction of such new materials in the aircraft structure and cabin could have.

The FSS P7 project is led by ONERA, as its experience covers both Crash and Fire worthiness of A/C composite materials and structures. ONERA also leads the first work package which aims at better understanding and characterizing the fire and high temperature behavior of primary structure CFRP materials. DLR leads the second work package which is dedicated to the improvement of current material solutions to mitigate fire, smoke and fumes in the cabin environment. Last, NLR leads the third work package the objectives of which are to study the indirect effects of such new materials, technologies and

fuel systems on the on-board aircraft air quality. Bridges between the different tasks and partners are implemented by CEIIA (WP 7.1 and WP7.3), VZLU (WP7.2) and Cranfield University (WP7. 1 and WP7.3), and access to the industry is reached in all tasks thanks to the contribution of Airbus-military (AIRBUS D&S, WP7.1), ALENIA (WP7.2) and EMBRAER (WP7.1 and WP7.3) companies. The overall project consistency will be increased by CAA UK providing regulatory advice and guidance to all the project tasks.

1.3. Research objectives

The objective of FSS P7 work package WP7.1 “Understanding and characterising the fire behaviour of primary structure composite materials (epoxy resins, standard CFRP)” is to enhance knowledge concerning the fire behaviour and performance of CFRP primary structure composite materials, in order to better predict safety and survivability issues in case of fire incident or post-crash situation. Such predictions rely on physical models and numerical tools which need to be developed based on exhaustive material (characterisation) and components (validation) experimental testing. The objective of WP7.1 is to produce a comprehensive experimental database for a reference material to be shared by the European research community as a basis for material model development of the fire behaviour and degradation of CFRP materials. The T700GC/M21 material has been proposed to be used in this WP7.1 because a lot of published results already exist about its standard mechanical behaviour which the project can build on.

Earlier work in FSS WP7.1 produced included a list of complementary tests which could be developed and performed to complete the already existing database with respect to:

- Mechanical and thermo-mechanical properties of virgin and charred material,
- Dynamic degradation phenomena (incl. ignition of combustible gases inside the CFRP laminate) during the fire exposure time,
- Fire resistance of damaged composite panels to direct exposure to flame impact.

This objective of this study is to present the test results from a first batch of T700/M21 test specimens.

1.4. Approach

The objective of WP7.1 is to enhance knowledge concerning the fire behavior and performance of CFRP primary structure composite materials, in order to better predict safety and survivability issues in case of fire incident or post-crash situation. Such predictions rely on physical models and numerical tools which need to be developed based on exhaustive material (characterization) and components (validation) experimental testing. The objective of WP7.1 is also to produce a comprehensive experimental database for a reference material to be shared by the European research community as a basis for material model development of the fire behavior and degradation of CFRP materials. The T700GC/M21 material has been proposed to be used in this WP7.1 because a lot of published results already exists about its standard mechanical behavior which the project can build on. Partners’ state-of-the-art models and simulation tools will be assessed according to this comprehensive set of experimental data. FSS P7 WP7.1 was split into 3 tasks:

- T7.1.1. Definition of tests, manufacturing of test coupons and panels, preparation of tests (incl. instrumentation), led by CeiiA (see deliverable FSS P7 D7.1)
- T7.1.2. Test and model the thermochemical, thermophysical and thermomechanical properties of composite materials according to temperature, fire exposure (time), and material state (virgin and charred), led by ONERA,
- T7.1.3. Test and model resilience to temperature/fire effects at structural levels (incl. on damaged panels), led by CASA.

The present FSS P7 D7.4 deliverable “Primary structure materials – Test results (first batch)” refers to task T7.1.2 of WP7.1.

1.5. Structure of the document

The introduction being done, the next sections of the document are sub-divided according to the following topics:

- Thermophysical properties (specific heat and thermal conductivity tensor) at the virgin state and as a function of temperature,
- Thermochemical properties characterising the transformation reactions the material undergoes as a function of temperature and associated energies involved in each reaction ;
- Experimental protocol definition to assess mechanical and thermo-mechanical properties as a function of temperature.

In the last past years, ONERA has developed a test facility to provide thermophysical properties characterisation of anisotropic materials. Especially, it can assess simultaneously the specific heat and the 3 main components of the thermal conductivity tensor as a function of temperature. It is based on thermographic measurements of the material thermal response subjected to a pure radiative laser heating. The test facility was carried out on the selected T700GC/M21 CFRP material studied in 2 stacking sequences to the identified properties at the virgin state (*i.e.* below glass transition and pyrolysis).

In precedent studies [5], the thermal degradation of epoxy matrix reinforced by carbon fiber composite materials has been performed at Onera. During these studies, three main chemical reactions have been identified: pyrolysis of the matrix, oxidation of the char produced by the pyrolysis of the matrix and oxidation of the fibres. To succeed in, TGA and DSC experiments have been carried out in order to identify a thermal degradation model adapted to composite material. In this deliverable, only the first TGA results for the material manufactured and provided by CEiiA are presented. A discussion on the characterisation of the “volume” oxidation versus “surface” oxidation is also proposed.

A last set of preliminary results of the project is also presented in the document: as an example there is currently a lack of well-established protocols to assess the evolution of the mechanical properties (especially in terms of compressive properties which may be important for structural strength and

Project: Mitigating risks of fire, smoke and fumes
Reference ID: FSS_P7_ONERA_D7.4
Classification: Public



evacuation) and the degradation products (for short and long term exposition of paxs or cabin crew) of CFRP materials with the increase of temperature from ambient to above T_g . Original experimental protocols have been derived from ASTM or AFNOR standards and preliminary tests performed on T700GC/M21 (a well-spread material case study) CFRP specimens, will be presented in the document.

2 MATERIAL

The study is focused on one material used in the aeronautical industry for primary and secondary aircraft structures. The T700GC/M21 is a composite laminate made of carbon fibres (T700GC by TORAY) and epoxy resin reinforced by thermoplastic nodules (M21 by HEXCEL).

Plies of M21 / 35% / 268 / T700GC unidirectional, 260 μm -thick, prepregs are stacked and cured to provide the different composite laminates studied hereafter.

The material density is given at the virgin state: $\rho = 1580 \text{ kg/m}^3$.

Fibres average diameter is 7 μm and the volume fraction of fibres is 0.567 for the cured material. The final laminate thickness is about 2.08 – 2.10 mm for 8 ply laminates and 4.16 – 4.20 mm for 16 ply laminates.

CEiiA was in charge of manufacturing T700GC/M21 plates for ONERA. They were provided to ONERA in December 2015.

3 THERMAL CONDUCTIVITY TENSOR AND HEAT CAPACITY

3.1. Experimental method

3.1.1. BLADE facility description

The BLADE facility named from the French "Banc Laser de cAractérisation et de DEgradation" (characterisation and decomposition laser facility) and presented in Figure 1, is devoted, firstly, to the characterisation of thermo-physical properties of anisotropic materials [3] and secondly, to the analysis of the thermal response during decomposition of charring materials [4].

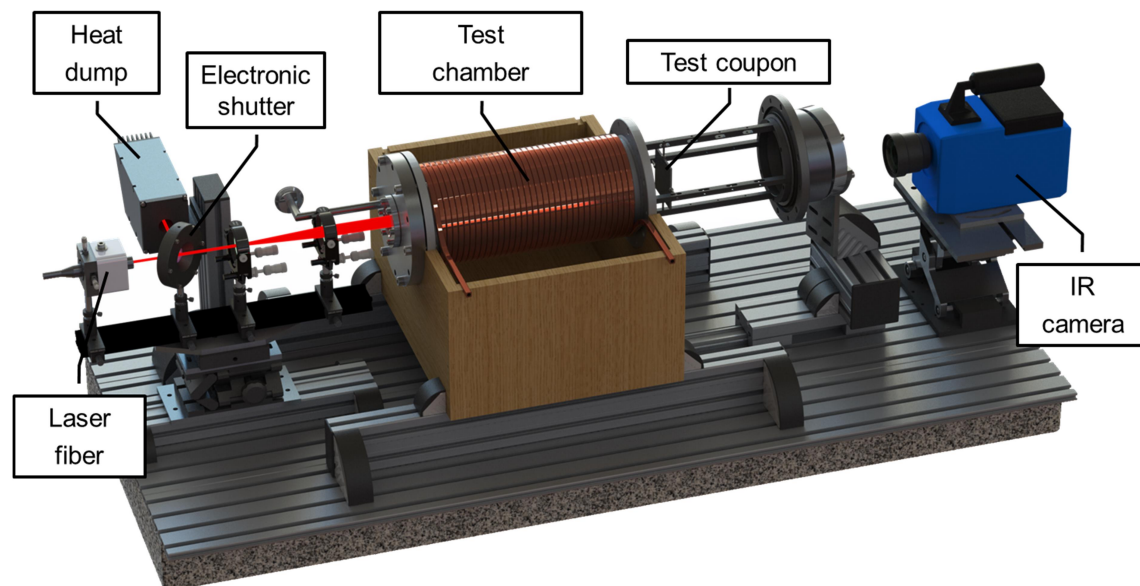


Figure 1 - Illustration of the BLADE facility: setup and instrumentation

Even if the apparatus is original, its principle is simple (Figure 2). A square-shaped ($80 \times 80 \text{ mm}^2$) test coupon is located within an air-filled pressure- and temperature-regulated test chamber. The specimen holder consists of 4 small nylon screws for the coupon to stand up straight with minimum contact and thermal loss by conduction. A continuous laser is used to heat up the front side of the test coupon. The laser generates a Gaussian monochromatic beam at the wavelength of $\lambda = 1080 \text{ nm}$, collimated at $\varnothing = 21.8 \text{ mm}$ at $1/e^2$ and with a maximum power of 50 W . The exposure time is accurately controlled with an electronic reflective shutter the diaphragm of which either directs the beam towards a heat dump or opens to heat the coupon up. The transient temperature at the back (unheated) side of the test coupon is measured using quantitative infrared thermography from the test coupon at the initial cold temperature, then during the heating phase up to the cooling phase when the shutter diaphragm is closed and the laser switched off.

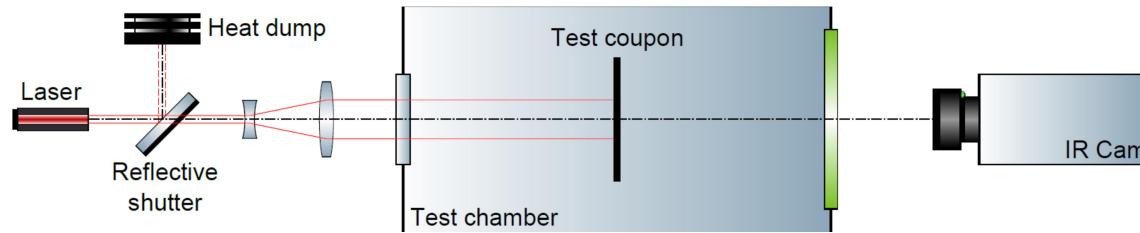


Figure 2 - Principle of the experiments: thermo-physical characterisation and laser-induced decomposition of charring materials

A key feature of the apparatus is an accurate control of the test conditions with respect to some conventional standard tests. The temperature regulation is applied to the chamber outer cylindrical surface using a coolant fluid flowing through a copper tubing coil. The heat transfer from the coil to the chamber is governed by conduction: a thermally conductive compound ensures a good contact and glass wool (not represented in Figure 1) isolates the test chamber from the surrounding environment. Within the test chamber, the temperature regulation of the test coupon is governed only by radiation. The inner surface of the test chamber is coated with a high emissivity black paint to maximise the exchanges. Moreover, the internal pressure is decreased by a vacuum pump that runs continuously during the experiments. The nominal value is set down to 5 *mBar* (500 *Pa*) which is low enough to avoid any convective heat transfer and prevent volatiles from flaming. Indeed, the determination of the convective heat transfer coefficient would have been very difficult even in a simple geometrical configuration. Moreover, constant values or conventional correlations may not be representative enough to model the convective exchanges with the surrounding environment either for natural convection or forced convection if an exhaust hood is used.

Another key feature of the BLADE facility consists in using a laser instead of a flame to heat the coupon up during the experiment. As mentioned in the introduction, fire is a complex phenomenon and the heat flux magnitude and distribution on the material exposed surface may be very difficult to assess accurately and reliably. Instead, the laser provides a heat source, stable in space and time, and characterised experimentally preliminary to the tests. The Gaussian distribution of the beam creates a non-uniform heating on the exposed surface which helps revealing the anisotropic behaviour of such composite laminates.

3.1.2. Measurement technique

The temperature measurement is based upon the quantitative infrared thermography technique included in the BLADE facility. The infrared camera is a FLIR SC7210 equipped with a mid-wave [3 – 5 μm] high sensitivity InSb detector, 320 \times 256 *pixels* resolution, low noise and high dynamic range. The camera offers an accurate external triggering feature which allows synchronisation of the image capture to other external devices such as the electronic shutter.

With respect to the expected temperature increase on the back surface of the test coupon, different integration times are used with specific calibrations for each temperature range to cover accurately the behaviour of the material with a reliable temperature resolution. The accuracy is given at $\pm 1^\circ\text{C}$ of the temperature expressed in $^\circ\text{C}$ between $[0 - 100^\circ\text{C}]$ and $\pm 1\%$ above. The reconstruction of the instantaneous camera images is then processed from the data at the four integration times to assess for each pixel of the field of interest the right temperature according to its range.

The acquisition frequency is 50 Hz ; consequently, the time period between each reconstructed image is 0.02 s .

The thermal analysis only relies on this technique for the measurements to remain non-intrusive, and for the test conditions at the material surfaces to be well-known.

3.1.3. Inverse heat conduction method for the laser source characterisation

The heat flux generated by the laser is assessed preliminary to the decomposition experiments by a non-linear inverse heat conduction method developed at ONERA [2011_Reulet]. The identification requires that all boundary conditions but those at the front (exposed) face are well-known as well as the material thermo-physical properties. In this respect, a pure titanium reference coupon coated with a high emissivity black paint ($\varepsilon = 0.96$) is used in the BLADE facility to provide accurate infrared thermography measurements.

The properties of the reference coupon are given in Table 1.

Temperature [$^\circ\text{C}$]	Temperature [K]	Thermal expansion coefficient [$1/\text{K}$]	Density [kg/m^3]	Specific heat [$\text{J}/\text{kg}/\text{K}$]	Thermal diffusivity [m^2/s]	Thermal conductivity [$\text{W}/\text{m}/\text{K}$]
23	296.15		4501	509	8.64E-06	19.79
70	343.15	1.01E-05	4495	529	8.04E-06	19.12
120	393.15	1.00E-05	4488	551	7.58E-06	18.74
200	473.15	9.90E-06	4478	590	7.00E-06	18.49
300	573.15					18.42
Uncertainty (k=2)		[$1/\text{K}$]	[$\%$]	[$\%$]	[$\%$]	[$\%$]
		7.00E-07	1	4	5	6
Dimensions	80 x 80 x 1	[± 0.015]				

Table 1 - Properties of the pure titanium reference coupon

The inverse method relies on a dedicated 3D Cartesian grid based heat conduction solver for homogeneous materials. The transient heat flux distribution is identified using data compression and filtering by a 2D discrete cosine transform and Beck's sequential method [1985_Beck] with the use of future time steps in order to minimise the difference between measured and calculated back temperatures in the least square sense. The inverse method is integrated in Onera's software THIDES, which also includes the direct thermal model. The direct model solves the non-linear heat conduction equation with a linearized scheme. The heat conduction equation is discretized with an ADI (Alternate Direction Implicit) finite difference scheme, modified to correct the instability of classical 3-D schemes.

Three tests are conducted on the titanium reference coupon and the thermal response is measured for the laser set at a given power. For thermal properties assessment, the power is set low ($\sim 5 W$) in order to provide a moderate thermal loading on the coupon to be characterised. The tests are performed on different hours and days for stability and repeatability of the laser operation to be evaluated.

The test matrix with detailed test conditions is presented in Table 2:

<i>Test #</i>	<i>T_{chamber} [°C]</i>	<i>I_{laser} [A]</i>	<i>t_{laser} [s]</i>	<i>t_{acq} [s]</i>	<i>f_{acq} [Hz]</i>	<i>T_{atm} [°C]</i>
001	22	12	5	10	50	23.1
002	22	12	5	10	50	23.2
003	22	12	5	10	50	23.5

Table 2 - Test matrix for the laser source characterisation

The first results concern the estimation of the heat flux density by the inverse heat conduction method. They are presented in Table 3 for the 3 repeatability tests. The comparison of the maximum heat flux density provided by the laser for each test shows very similar values with a magnitude of $26 kW/m^2$. Integration over the material surface is then performed to assess the total power supplied by the laser. Values of about $4.7 W$ are calculated with a maximum relative error of 0.4 %. The difference between the theoretical value of $5 W$ and the calculated values of $4.7 W$ corresponds to transmission factor of the access window of the laser.

As a consequence, accuracy and repeatability of the global results are very satisfying to assess the thermal loading provided by the laser source.

Test #	$\Phi_{laser}^{max} [W/m^2]$	$P_{laser} [W]$	$(P_{laser} - \langle P_{laser} \rangle) / \langle P_{laser} \rangle [\%]$
001	26135	4.748	+0.40
002	26114	4.722	-0.15
003	26117	4.717	-0.25

Table 3 – Comparison of maximum heat flux densities and integrated powers

However, the time and space distribution is required for the properties assessment. Figure 3 shows the detailed results of the inverse heat conduction method at $t = 5 s$ of test #003.

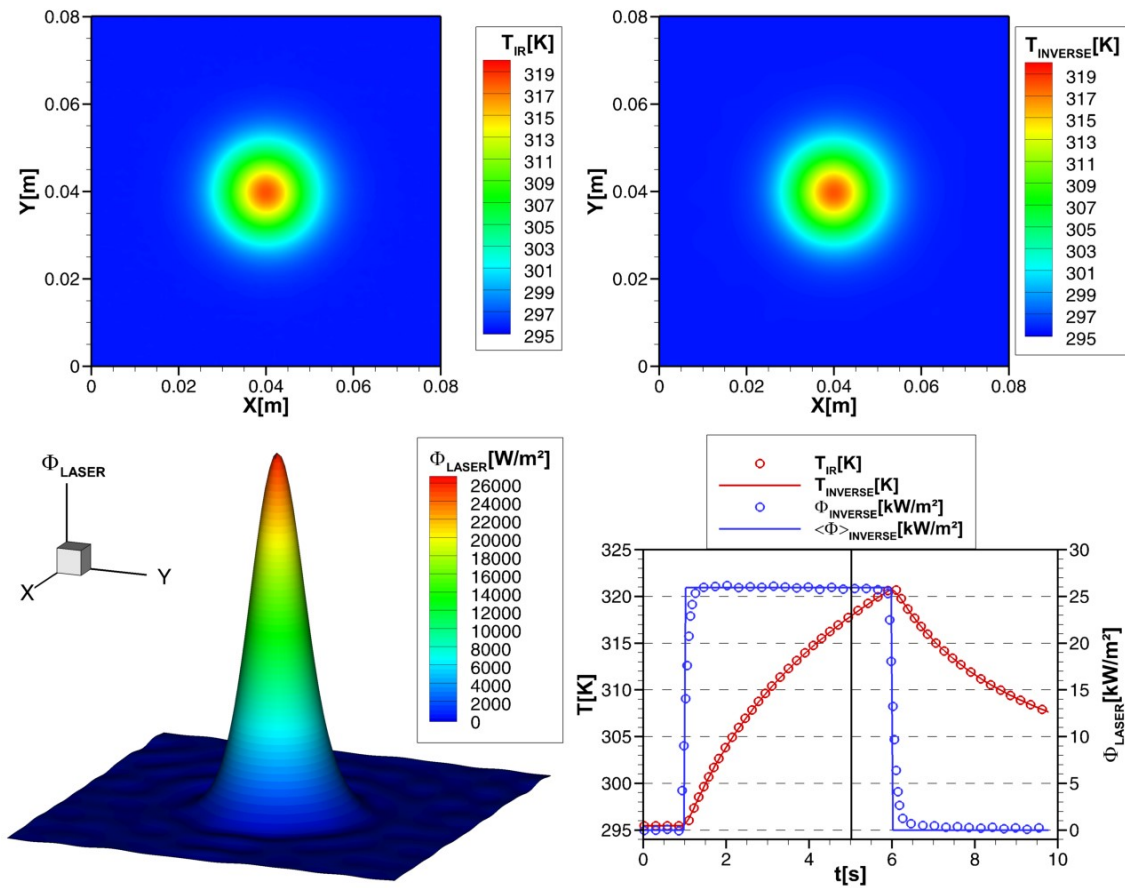


Figure 3 - Results of the inverse heat conduction method for test #003 at $t = 5 s$

The temperature map measured by the infrared thermography on the back surface of the titanium material is plotted on the upper left side. The associated temperature map calculated by the inverse method is plotted on the upper right side at the same moment of the experiment. The first shows high quality temperature measurements with very low noise while the second shows identical thermal response calculated by the method.

The accuracy of the results is confirmed on the curves plotted on the lower right side of Figure 3 where temperature and heat flux are extracted over time at the centre of the surface results. The inverse temperature ($T_{inverse}$) perfectly fits the measured temperature (T_{IR}). The use of future time steps in the inverse method induces a smoother ramp on the heat flux identification ($\Phi_{inverse}$) but the result is very stable in time during the laser operation as expected.

Finally the heat flux distribution identified by the inverse method is plotted on the lower left side and coloured by heat flux contours. The Gaussian distribution of the laser beam is estimated with a high accuracy to provide the boundary condition required on the exposed surface of the coupon to be characterised.

Very similar results are obtained from the two first tests and are not presented here.

3.1.4. Global thermophysical properties assessment of homogenised orthotropic composite materials

The same test conditions and laser settings are applied for the assessment of the thermophysical properties of the composite materials. With the heat flux previously identified by the inverse heat conduction method, all boundary conditions are known to perform the characterisations. The pure titanium reference coupon is simply replaced by a composite coupon. The new inverse problem consists in identifying the specific heat and the thermal conductivity tensor simultaneously. The conductivity tensor is only composed of the diagonal components since thermal diffusion within the test coupons is orthotropic for the considered UD and QI layouts.

The problem resolution is based on the transient temperature maps measured by IR thermography: $T_{i,j}^{[t]}_{IR}$; where (i, j) subscripts refer to space coordinates of the back surface grid cells and $[t]$ superscript refers to the time variable associated to the acquisition period.

Then, properties initialisation (all properties set to 1) is performed. The problem unknowns are formulated by the “properties vector”:

$$Properties = [C_p^{(0)}, C_p^{(1)}, k_x^{(0)}, k_x^{(1)}, k_y^{(0)}, k_y^{(1)}, k_z^{(0)}, k_z^{(1)}]^T$$

corresponding to the polynomial coefficients of the thermophysical properties of the material. These 8 parameters define the thermal behaviour laws of the properties assuming a linear evolution on the considered temperature range. Higher order polynomial behaviour can be assessed by a piece-wise linear approach.

The temperature dependency is granted both by the temperature evolution within the coupon during the test and by the input measurements performed at different initial temperatures within the range of the BLADE facility: $[0 - 100 \text{ }^\circ\text{C}]$ provided by the thermal regulation of the test chamber.

The Levenberg-Marquardt iterative optimisation method is used to minimise the difference between the measurements and the calculated transient temperature maps $T_{i,j}^{[t]}_{OPT}$ as represented in Figure 4.

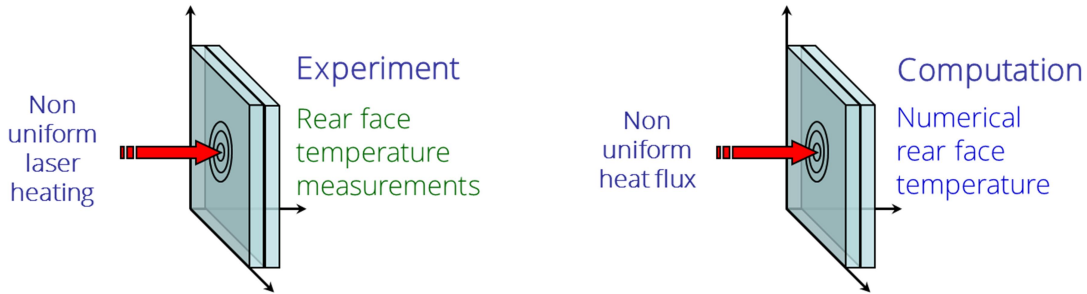


Figure 4 - Inverse method principle for thermophysical properties assessment

The difference is expressed by the objective functional in the least square sense:

$$Functional = \sum_i^{n_x} \sum_j^{n_y} \sum_t^{n_t} [T_{i,j}^{[t]} - T_{i,j}^{[t]}(Properties)]^2$$

where (n_x, n_y, n_t) are the number of grid cells in the x and y direction respectively and the number of time steps.

The iterative algorithm is detailed in Figure 5 and runs until convergence to get the thermophysical properties of the material.

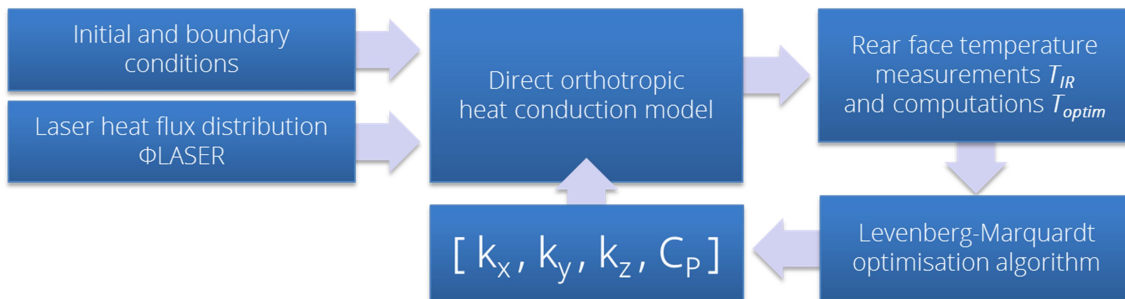


Figure 5 - Iterative algorithm of the inverse method for thermophysical properties assessment

3.2. Results overview and global properties analysis

3.2.1. Preparation of the test coupons

The specimens tested in the BLADE facility and presented in this study are prepared and conditioned from the panels provided by CEiiA. Water jet cutting is used to prepare the test coupons to the required dimensions for the BLADE facility.

The coupons can be seen in Figure 6. One surface is smooth while the other is rough due to the manufacturing process.

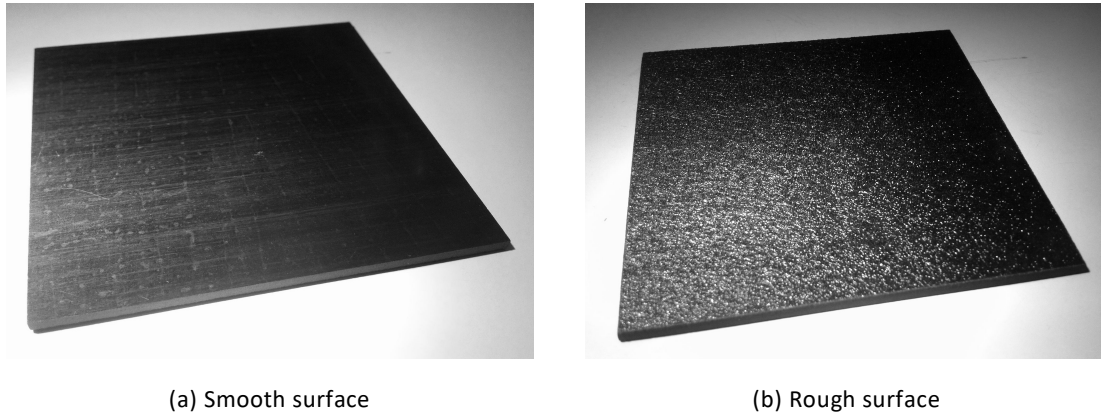


Figure 6 - Water jet cut test coupons

One panel is used for each layout to assess the thermophysical properties of the material. The associated references are given in Table 4:

Coupon reference	Stacking sequence	Dimensions
3809A_FSS_P7_P208-01_SS02#01	$[0]_8$	$80 \times 80 \times 1 \text{ mm}^3$
3809A_FSS_P7_P227-01_SS06#01	$[45/90/-45/0]_s$	$80 \times 80 \times 1 \text{ mm}^3$

Table 4 - Reference of the test coupons

The stacking sequence of the quasi-isotropic (denoted QI) coupons is: $[45/90/-45/0]_s$

The stacking sequence of the unidirectional (denoted UD) coupons is: $[0]_8$

For all the tests presented hereafter, the infrared thermography is performed on the smooth surface of the material. As a consequence, the heat flux generated by the laser is applied on the rough surface.

3.2.2. Test matrix

The test matrix for the thermophysical properties assessment consists in performing 3 repeatability tests for each temperature applied on the test chamber. Four temperature levels are chosen within the operating range of the BLADE facility. The magnitude of the temperature evolution measured on the back surface of the test coupons is about 20 °C during the experiments. As a consequence, the temperature dependency is assessed by increasing the temperature of the test chamber by 20 °C between each series of tests.

The test matrix is detailed in Table 5.

<i>Test #</i>	<i>Stacking sequence</i>	$T_{chamber}$ [°C]	I_{laser} [A]	t_{laser} [s]	t_{acq} [s]	f_{acq} [Hz]	T_{atm} [°C]
004	UD	22	12	5	30	50	22.6
005	UD	22	12	5	30	50	22.8
006	UD	22	12	5	30	50	23.0
007	UD	40	12	5	30	50	23.8
008	UD	40	12	5	30	50	24.3
009	UD	40	12	5	30	50	24.1
010	UD	60	12	5	30	50	24.6
011	UD	60	12	5	30	50	24.9
012	UD	60	12	5	30	50	25.3
013	UD	80	12	5	30	50	25.3
014	UD	80	12	5	30	50	25.7
015	UD	80	12	5	30	50	26.2
016	QI	22	12	5	30	50	25.1
017	QI	22	12	5	30	50	25.2
018	QI	22	12	5	30	50	25.3
019	QI	40	12	5	30	50	26.1
020	QI	40	12	5	30	50	26.3
021	QI	40	12	5	30	50	26.4
022	QI	60	12	5	30	50	23.4
023	QI	60	12	5	30	50	24.0
024	QI	60	12	5	30	50	24.3
025	QI	80	12	5	30	50	25.7
026	QI	80	12	5	30	50	26.1
027	QI	80	12	5	30	50	26.2

Table 5 - Test matrix for the thermophysical properties assessment

3.2.3. Test protocol

They are placed successively within the test chamber regulated at the initial temperature (T_{chamb}) and the pressure is lowered down to 5 mBar for all the experiments. Temperature stabilisation of the specimens is ensured before each test to begin. It is essential to note that the thermal exchanges with the chamber only result from radiative heat transfer not only initially but also during the whole test since convective heat transfer is avoided. The orientation of each test coupon in the experiment is precisely performed by aligning the fibre direction of the first ply of the laminate along the horizontal direction.

The test protocol is illustrated in Figure 3. It simply consists in running the IR acquisition 1 s before subjecting the specimen to the laser heat flux during 5 s. The laser generates a constant, steady but non-uniform heat flux that creates a thermal loading locally on the centre of the material front surface. Finally, the IR camera keeps on measuring the temperature up to $t = 30$ s while the laser is switched off and the test coupon is cooling down thanks to radiative exchanges with the chamber.

3.2.4. Optimisation process

It is important to notice that both the heating phase and the cooling phase are important in the optimisation process because the first is relevant to the thermal response during the laser exposure and the second is relevant to thermal losses due diffusion within the material and radiation with the test chamber. Agreement on both phases ensures a good accuracy considering the thermal loading and boundary conditions.

Input data for the optimisation process to assess the thermophysical properties are then a couple of tests performed at different initial temperature. The material density is assumed to be known at the given value: $\rho = 1580 \text{ kg/m}^3$. The test coupon exact dimensions are used to model the material numerically. The computational grid is based on the pixels distribution of the region of interest the IR images to model the material surface. The grid is then extruded in the through-thickness direction with a number of cells calculated with respect of a relevant Fourier number to ensure stability of the computation with the direct heat conduction solver THIDES.

Temperature dependency is evaluated with different choices for the couples of tests. The thermal behaviour laws are then calculated on the whole temperature range available with the BLADE facility from the batch of optimisation computations.

The computation matrix for the optimisation process is given in the next sections for each material configuration: UD8 and QI8.

One optimisation computation with a couple of test results takes about 8 to 10 hours of CPU-time to converge to the right thermophysical properties. As a consequence, all tests detailed in Table 5 have not been used to assess the properties. Instead, repeatability is evaluated from the 3 test results performed at the same initial temperature. And then, one out of the three tests is used for each initial temperature condition. As a result, only 4 tests are used for the optimisation process for each test coupon.

The resulting computational matrix is given in the next sections of each configuration.

3.2.5. Thermophysical properties of the unidirectional composite laminate

As for the heat flux identification, the repeatability of the experiments with composite test coupons is very satisfying with identical temperature evolution on the back surface. As mentioned in the previous section, the needed number of test results can be limited to one for each initial temperature condition. The resulting matrix is given in Table 6.

<i>Test #</i>	<i>Stacking sequence</i>	$T_{chamber}$ [°C]	I_{laser} [A]	t_{laser} [s]	t_{acq} [s]	f_{acq} [Hz]	T_{atm} [°C]
006	UD	22	12	5	30	50	23.0
009	UD	40	12	5	30	50	24.1
012	UD	60	12	5	30	50	25.3
015	UD	80	12	5	30	50	26.2

Table 6 - Tests used for the identification of the thermophysical properties of the T700GC-M21-UD8 composite laminate

Considering the complete test matrix would not add any information in the optimisation process since the thermal response does not vary if the material is subjected to identical test conditions (heat flux and test environment).

However, the temperature dependency is calculated on different temperature ranges to evaluate if the thermal behaviour law remains linear as a function of temperature. The computational matrix is composed of 5 series of optimisation runs on 5 different temperature ranges as detailed in Table 7.

<i>Optimisation computation runs #</i>	<i>Couple of tests #</i>	<i>Temperature range of the identification [°C]</i>
1	006-009	22-40
2	009-012	22-60
3	009-012	40-60
4	009-015	40-80
5	012-015	60-80

Table 7 - Computational matrix for the identification of the thermophysical properties of the T700GC-M21-UD8 composite laminate

The following figures show the results of the optimisation runs and compare the temperature map measured by the infrared thermography (T_{IR} on the left) and the temperature map calculated by the numerical solver with the optimal properties (T_{OPTIM} in the middle). The measurements are of course

noisier than the computations. Both maps are plotted at $t = 10$ s to show significant heat transfer on the material back surface. On the right of each figure, temperature is extracted over time at the centre of the maps and plotted in red and blue lines while the relative error is plotted in green.

The Figure 7 shows the results for the first optimisation run considering the temperature range $[22 - 60\text{ }^\circ\text{C}]$. The Figure 7(a) shows the results for TEST #006 while the Figure 7(b) shows the results for TEST #009. Both thermal responses issued from the optimal process (T_{OPTIM}) are calculated with the same thermophysical properties assuming a linear behaviour of the specific heat and the thermal conductivity. It is important to notice again that firstly, 2 polynomial coefficients are identified for each property and secondly, the thermal conductivity is specified with 3 different components to account for the orthotropic behaviour of composite laminates. As a consequence, 8 unknown parameters have to be identified by the optimisation process for each couple of tests.

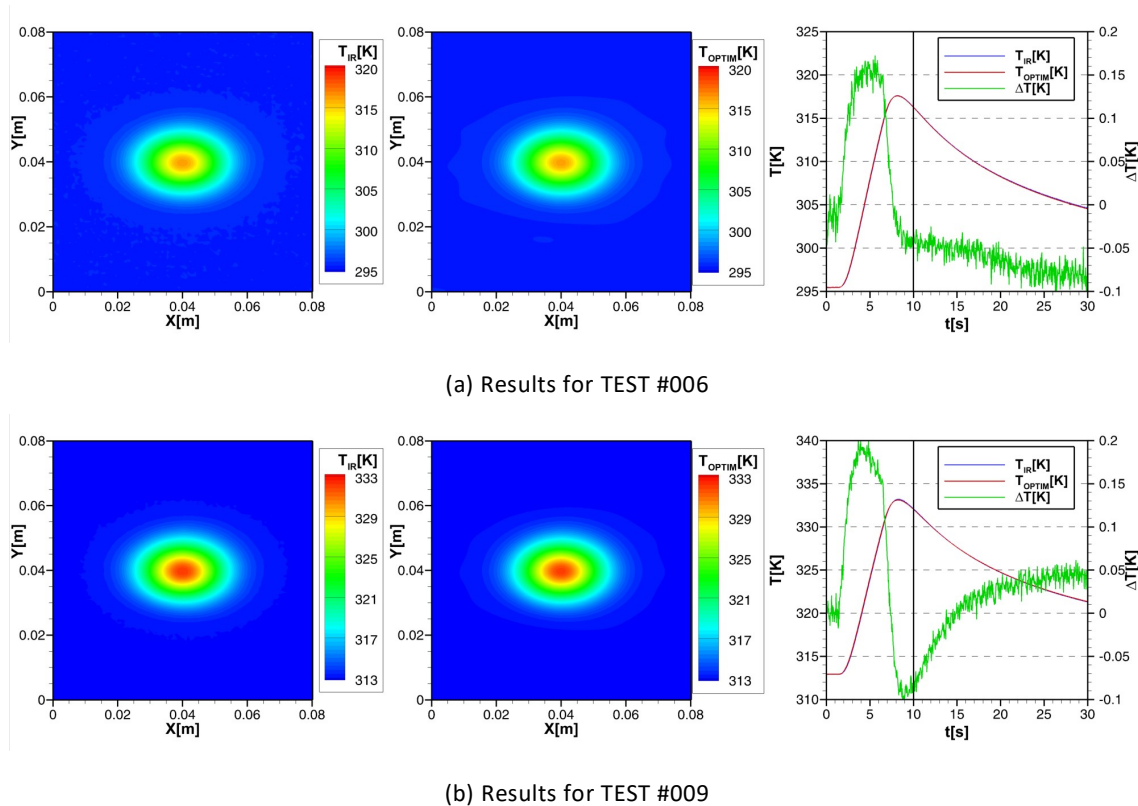


Figure 7 - Results comparison for the optimisation run #1 on the temperature range $[22 - 40\text{ }^\circ\text{C}]$ for T700GC-M21-UD8

The experimental results in Figure 7 exhibit that the thermal response of the unidirectional composite laminate is anisotropic with preferential heat transfer along the fibres direction. It is important to recall that the 0° -orientation is aligned with the horizontal direction. The heat flux provided by the laser on the

front surface is axisymmetrical but the fibres alter the heat diffusion within this heterogeneous medium and result in an ellipsoid thermal response on the back surface.

The result of the optimal computation shows that the orthotropic modelling of the heat transfer can provide a satisfactory thermal response induced by the thermal loading generated by the laser. The temperature evolution is predicted with a very good accuracy with a maximum temperature error of $\Delta T = 0.02 K$ (green curve in Figure 7) for the considered couple of tests. The temperature evolution extracted over time at the centre of the back surface is identical in both the measurements and the optimal computation. The blue and red curves in Figure 7 are superimposed all along the experiment which means that the laser synchronisation and thermal test conditions have been provided to the computation with a very good accuracy.

Another interesting feature to notice is that the temperature evolution is different either the first test or the second test is considered. The magnitude of the temperature evolution (difference between the initial temperature and the maximum temperature) decreases from about $22^\circ C$ to about $20^\circ C$ if the initial temperature applied to the test chamber increases from $22^\circ C$ to $40^\circ C$. This feature is the signature of a change in the thermophysical properties as a function of temperature because the material does not behave the same way when subjected to the same heat flux on the exposed surface.

The Figure 8 shows the second optimisation run performed on a larger temperature range.

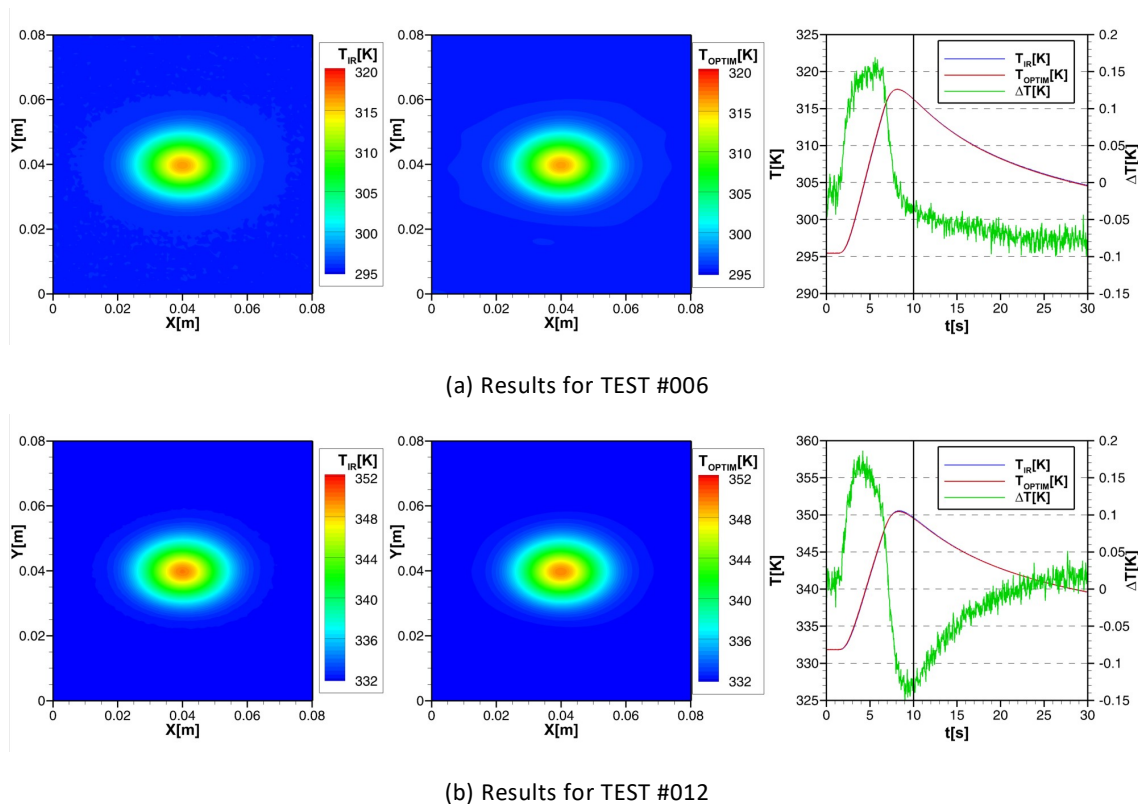


Figure 8 - Results comparison for the optimisation run #2 on the temperature range [22 – 60 °C]

The agreement between the measurements and the optimal computation remains very good with the same relative error on temperature. The magnitude of the temperature evolution at the centre keeps on decreasing (down to less than 20 °C) if the initial temperature is increased up to 60 °C in TEST #012. All properties (specific heat and diagonal components of the thermal conductivity tensor) must have changed with the increase of temperature but the thermal behaviour remains orthotropic.

Figure 9 to Figure 11 show the 3 last optimisation runs. The agreement remains satisfactory whatever the temperature range considered in the identification process. The repeatability of the experiment is granted for each temperature level applied to the test chamber. The temperature-induced evolution of the thermophysical properties is noticeable on the measurements comparison.

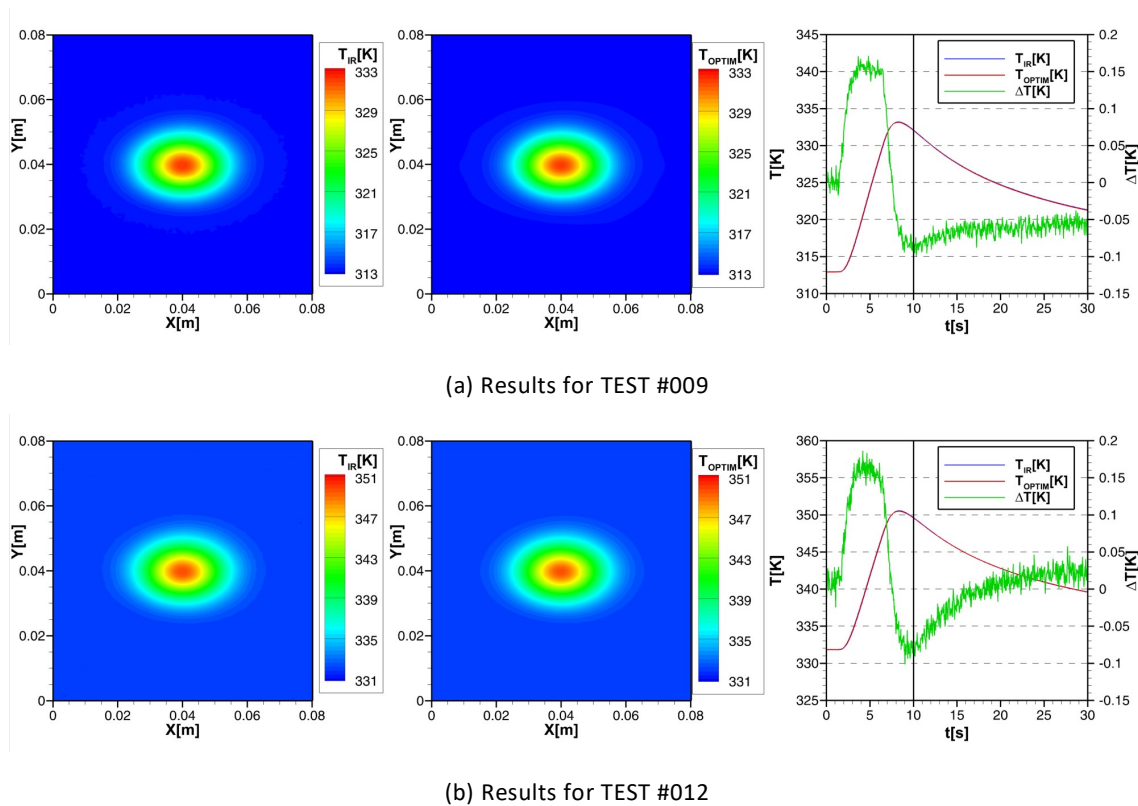
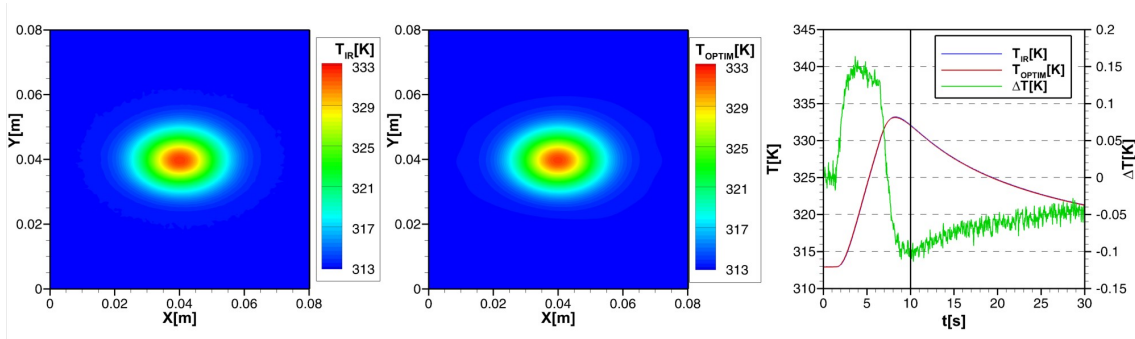
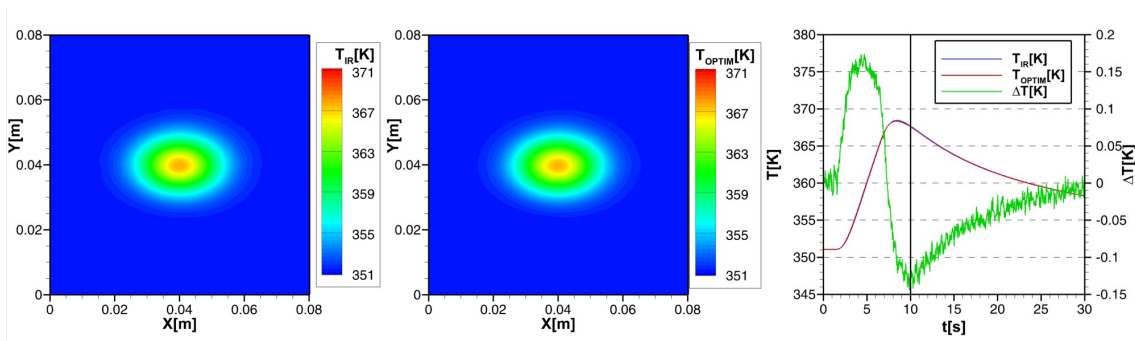


Figure 9 - Results comparison for the optimisation run #3 on the temperature range [40 – 60 °C]



(a) Results for TEST #009



(b) Results for TEST #015

Figure 10 - Results comparison for the optimisation run #4 on the temperature range [40 – 80 °C]

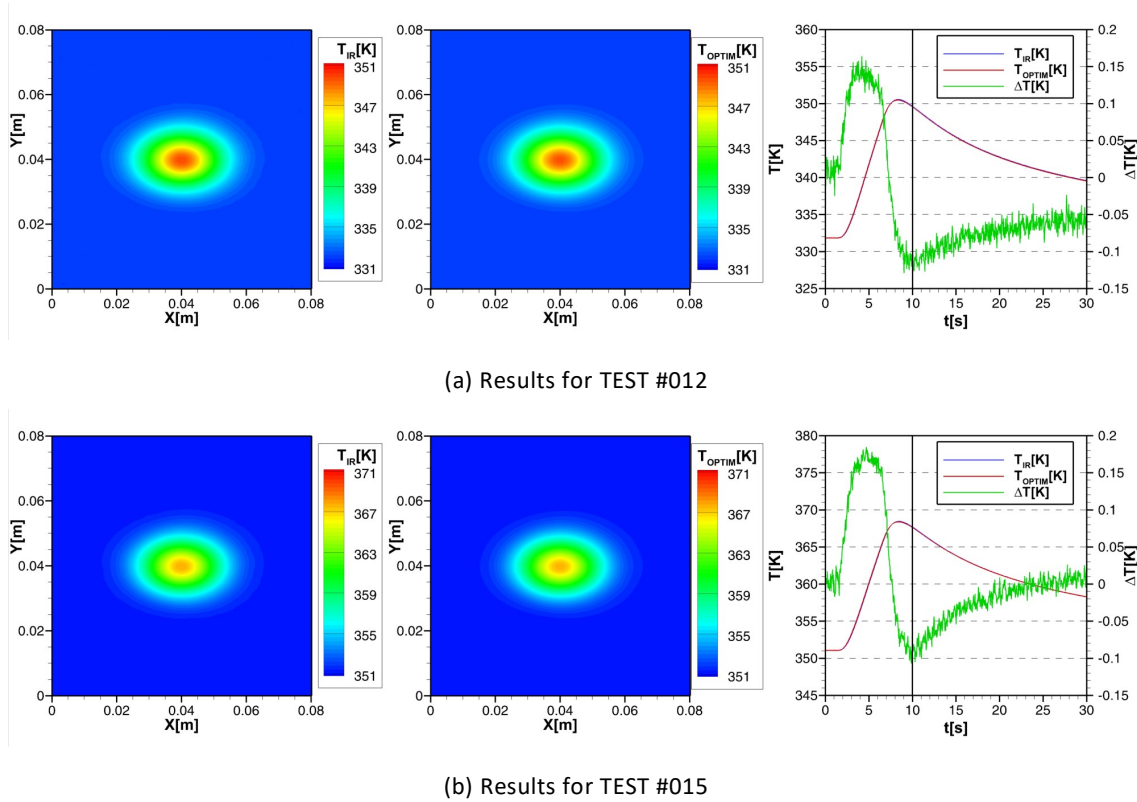


Figure 11 - Results comparison for the optimisation run #5 on the temperature range [60 – 80 °C]

The result of each optimisation run provides a first order polynomial expression for the thermophysical properties. The 4 properties are plotted from Figure 12 to Figure 15 with one line for each temperature range. The 20 °C-increase of temperature during each test is taken into account to extend the applicability of the thermal laws. As a result, each temperature range has a magnitude of 40 °C.

All properties increase as a function of temperature in the range of interest.

The specific heat is plotted in Figure 12. For the highest temperatures, the specific heat is more than 30 % higher than the value at room temperature. The temperature-dependency is then significant and cannot be neglected. The slope of the curves decreases as the temperature increases. The behaviour is not linear and an extrapolation of the law identified on the first run would have resulted in overestimated values of the specific heat at higher temperature. The different identifications are coherent with each other and the evolution of the specific heat seems continuous as a function of temperature.

The evolution of the 3 components of the thermal conductivity tensor is more complex to analyse. The thermal conductivity along the fibres direction (k_{xx}) is about 10 × higher than the thermal conductivity in the through-thickness direction (k_{zz}) considering the unidirectional stacking sequence of the laminate. Moreover, in-plane thermal conductivity components are also very different. In the transverse direction (k_{yy}), the discrepancies of the results from the 5 different optimisation runs are higher.

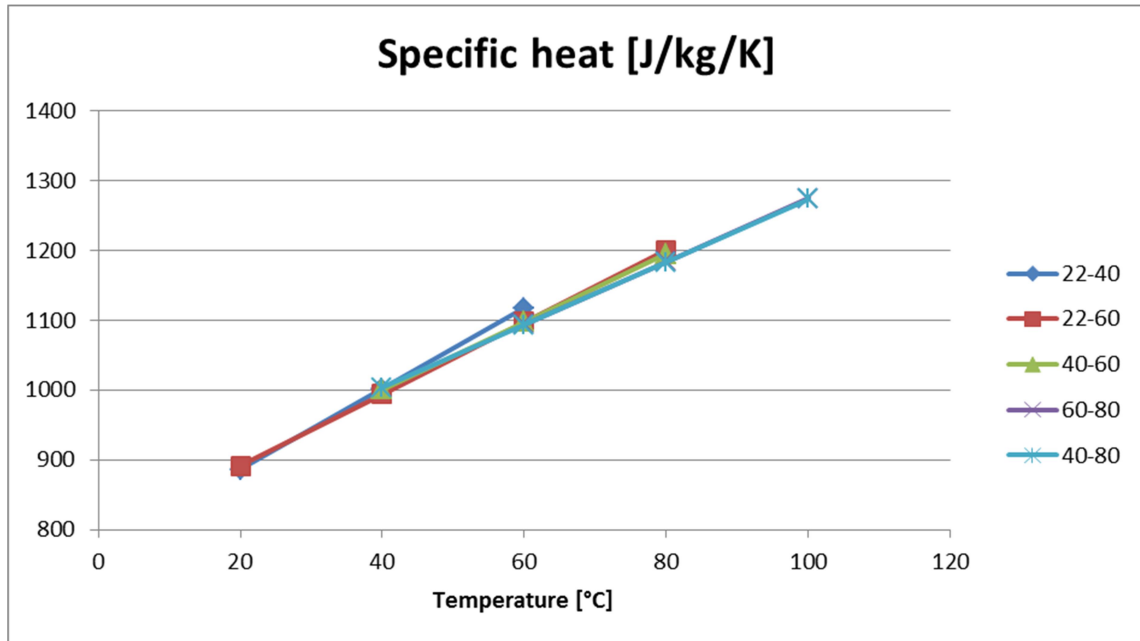


Figure 12 - Comparison of the specific heat identifications on the different temperature ranges for the T700GC-M21-UD8 composite laminate

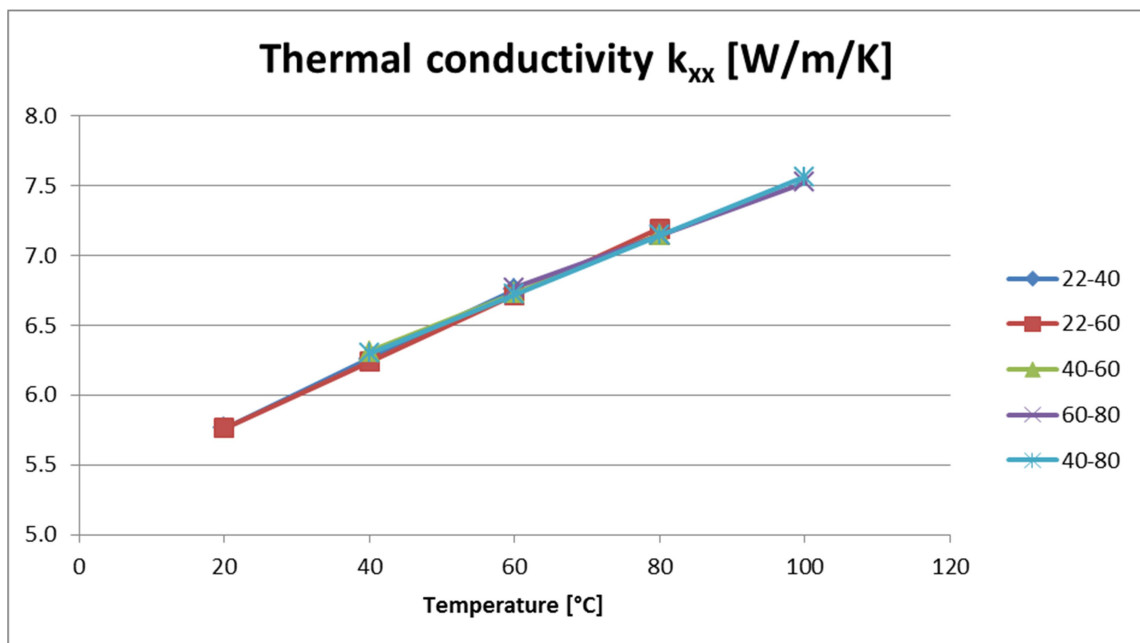


Figure 13 - Comparison of the thermal conductivity k_{xx} identifications on the different temperature ranges for the T700GC-M21-UD8 composite laminate

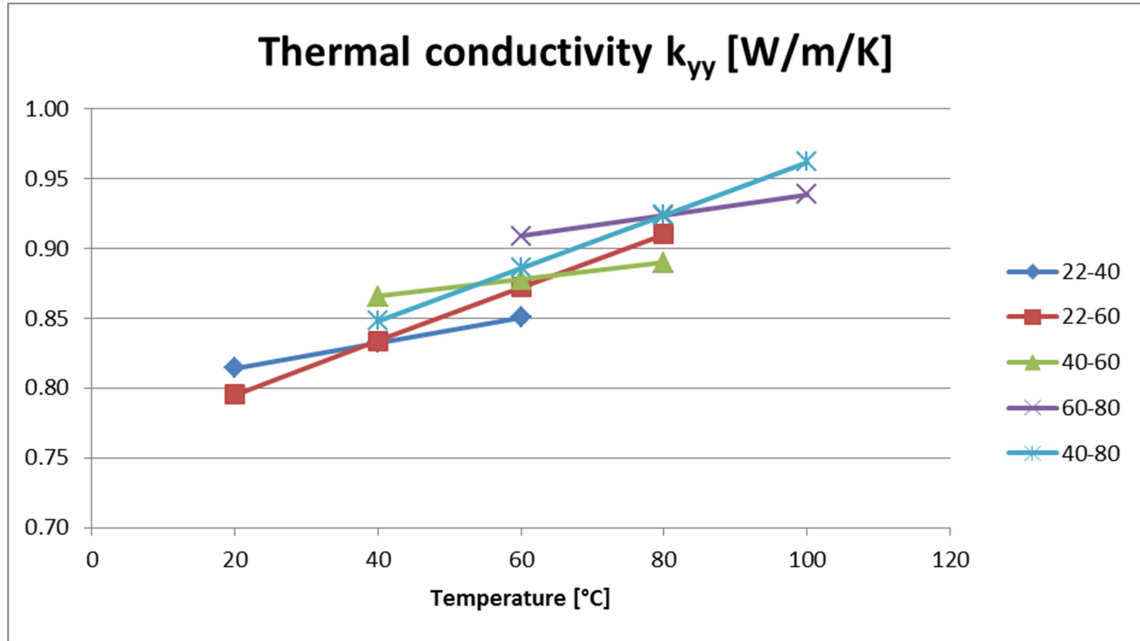


Figure 14 - Comparison of the thermal conductivity k_{yy} identifications on the different temperature ranges for the T700GC-M21-UD8 composite laminate

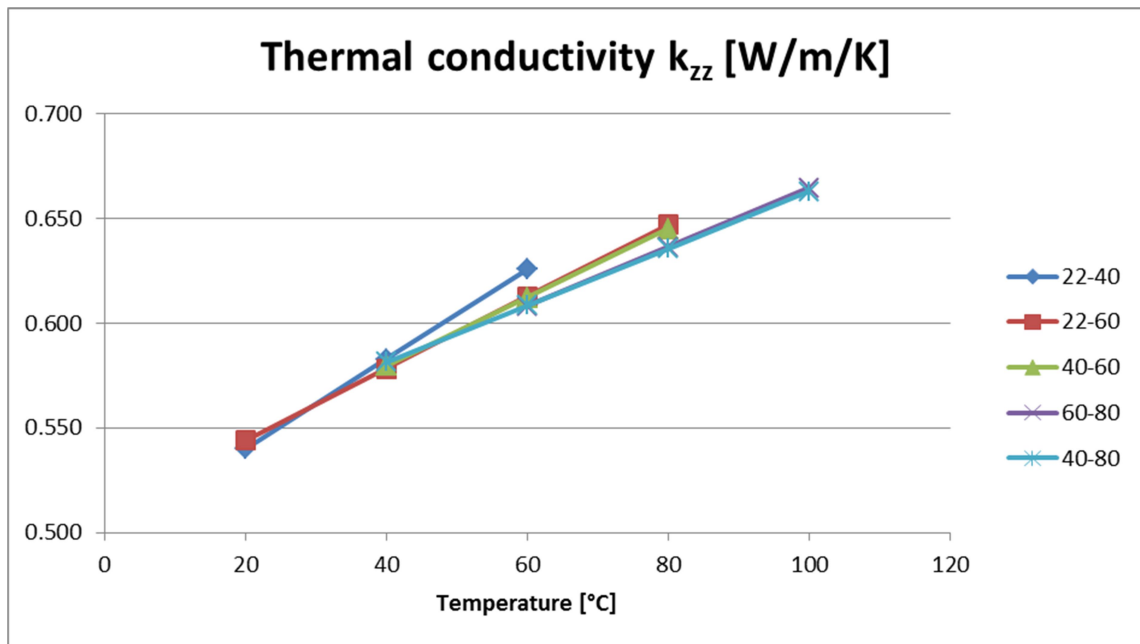


Figure 15 - Comparison of the thermal conductivity k_{zz} identifications on the different temperature ranges for the T700GC-M21-UD8 composite laminate

It is important to notice that k_{xx} and k_{yy} components are identified mainly from in-plane heat transfer measured by the infrared thermography. The third component in the through-thickness direction is identified from the time delay between the beginning of the laser operation at $t = 1$ s and the moment

when a temperature signal is measured on the back surface. A good synchronisation of the different signals is mandatory to assess accurate properties.

Considering the difference between the 2 in-plane components of the thermal conductivity tensor, the sensitivity of the identification method seems higher along the fibres direction than in the transverse direction. The temperature range considered in the optimisation process has a significant impact on the identified results for k_{yy} . The discrepancies are about $2 \times$ higher for the in-plane transverse component than for the others.

The other 2 components k_{xx} and k_{zz} have a more continuous evolution as a function of temperature. As noticed for the specific heat, the slope of the different curves is decreasing as the temperature is increasing.

An interesting feature is that k_{yy} and k_{zz} are different despite both are transverse to the fibres direction. Those two components should be equal according to the laminate theory. It may result from an interfacial effect caused a higher resin concentration in the interply interfaces than between fibres strands. As a consequence, the thermal conductivity component in the through-thickness direction has a lower value whatever the temperature value.

The thermal behaviour of the laminate is not linear as a function of temperature and higher order polynomial laws may be considered to assess a relevant temperature-dependency of the thermophysical properties. Figure 16 to Figure 19 shows a post-processing identification of the thermal laws on the whole temperature range from the previous piece-wise linear results. A second order polynomial law (in the plain black line) is compared to a first order linear law (in the plain red line). Both are fitted from the previous results plotted in blue symbols.

Considering the uncertainties and relative error obtained with the optimisation process from the IR measurements, the first order linear behaviour provides a satisfactory and relevant representation of the evolution of the properties on the temperature range of interest.

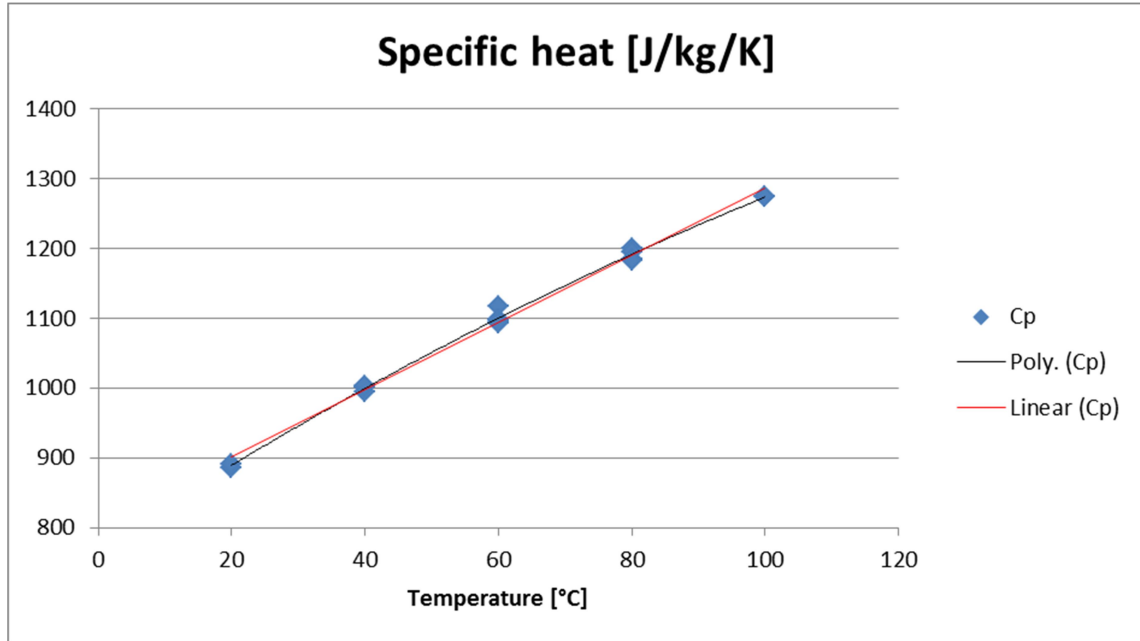


Figure 16 - Identification of the specific heat on the whole temperature range for the T700GC-M21-UD8 composite laminate

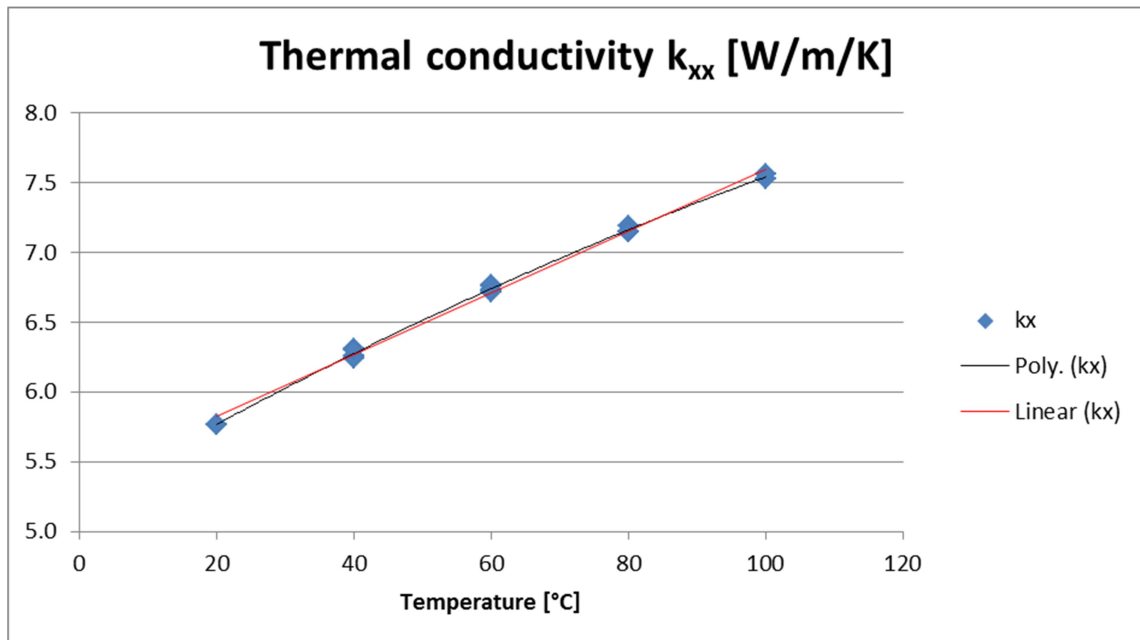


Figure 17 - Identification of the thermal conductivity k_{xx} on the whole temperature range for the T700GC-M21-UD8 composite laminate

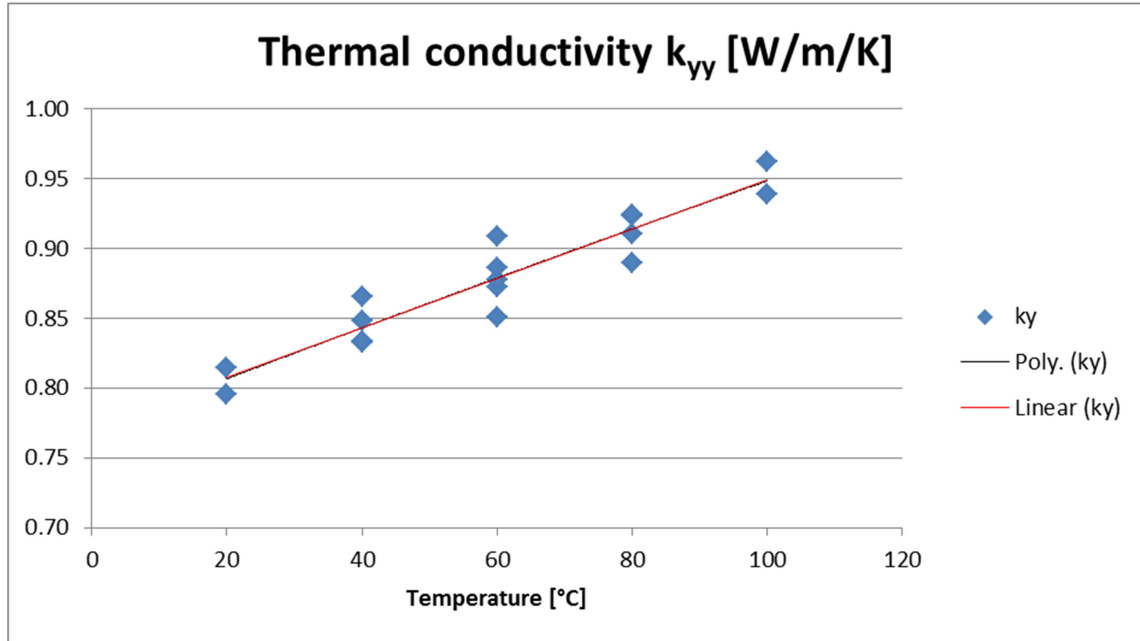


Figure 18 - Identification of the thermal conductivity k_{yy} on the whole temperature range for the T700GC-M21-UD8 composite laminate

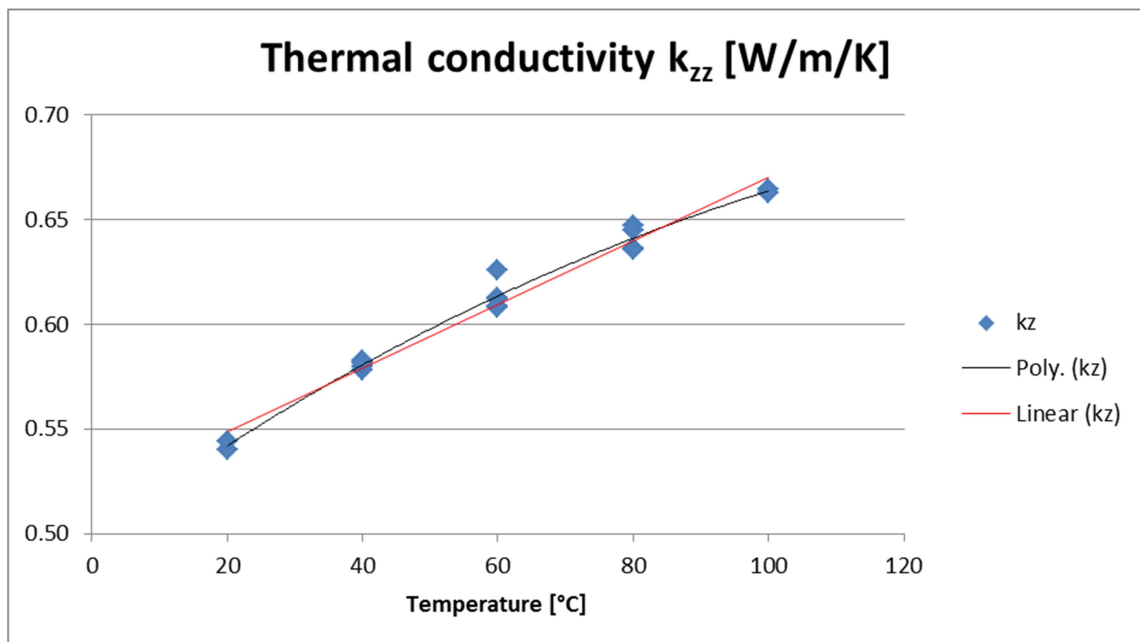


Figure 19 - Identification of the thermal conductivity k_{zz} on the whole temperature range for the T700GC-M21-UD8 composite laminate

The use of higher order polynomial laws should be done carefully because extrapolation beyond the temperature range used for the identification may result in non-physical results as presented in Figure 20. The decrease of the thermal conductivity at higher temperatures is not supported by any experimental result. It is the consequence of the second order polynomial evolution. **Additional results are required at higher temperatures to assess more accurate information about the temperature evolution of the thermophysical properties and avoid hazardous extrapolations.**

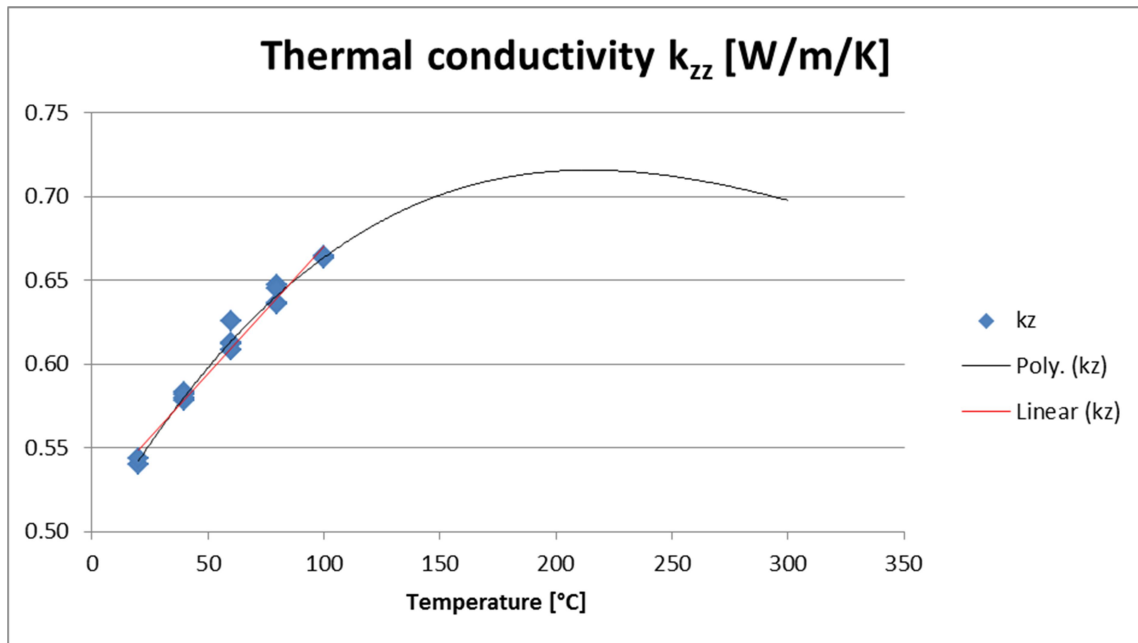


Figure 20 - k_{zz} property evolution at higher temperatures for the T700GC-M21-UD8 composite laminate

3.2.6. Thermophysical properties of the quasi-isotropic composite laminate

As for the unidirectional composite laminate characterisation, due to satisfactory repeatability of the experiments, the needed number of test results can be limited to one for each initial temperature condition. The resulting matrix is given in Table 8.

<i>Test #</i>	<i>Stacking sequence</i>	$T_{chamber}$ [°C]	I_{laser} [A]	t_{laser} [s]	t_{acq} [s]	f_{acq} [Hz]	T_{atm} [°C]
018	QI	22	12	5	30	50	25.3
020	QI	40	12	5	30	50	26.3
024	QI	60	12	5	30	50	24.3
027	QI	80	12	5	30	50	26.2

Table 8 - Tests used for the identification of the thermophysical properties of the T700GC-M21-QI8 composite laminate

The temperature dependency is calculated on different temperature ranges to evaluate if the thermal behaviour law remains linear as a function of temperature. The computational matrix is composed of 5 series of optimisation runs on 5 different temperature ranges as detailed in Table 9.

<i>Optimisation computation runs #</i>	<i>Couple of tests #</i>	<i>Temperature range of the identification [°C]</i>
6	018-020	22-40
7	018-024	22-60
8	020-024	40-60
9	020-027	40-80
10	024-027	60-80

Table 9 - Computational matrix for the identification of the thermophysical properties of the T700GC-M21-QI8 composite laminate

As presented in the previous section 3.2.5, the same plot layout is used to show the results for the quasi-isotropic composite laminate. Figure 21 to Figure 25 shows the comparison between the measured temperature (T_{IR}) and the temperature resulting from the optimisation process (T_{OPTIM}). The thermal response of the quasi-isotropic composite laminate is obviously isotropic in-plane compared to the previous stacking sequence. The measurements confirm that the fibres alignment direction has a significant effect onto the heat transfer within the material.

The repeatability of the experiment is granted for each temperature level applied to the test chamber.

The result of the optimal computations shows that the orthotropic modelling of the heat transfer can still provide a satisfactory thermal response induced by the thermal loading generated by the laser. The temperature evolution is predicted with a very good accuracy with a maximum temperature error of

$\Delta T = 0.04 K$ for the considered couple of tests. The relative error is twice than for the previous material configuration but the magnitude remains very low. The temperature evolution extracted over time at the centre of the back surface is very similar if the measurements and the optimal computations are compared. Some discrepancies can be noticed when the maximum value of the temperature is reached. The optimal computations slightly overestimate the increase of temperature at the centre of the back surface. However, the overall temperature evolution is closely captured by the optimisation process that provides the best set of material properties considering the associated measurements and the number of degrees of thermal freedom. The material behaviour can slightly differ from a pure orthotropic behaviour. Temperature dependency of the thermophysical properties can be observed from the results with a decrease of the maximum magnitude of the temperature evolution during the experiments when the test chamber temperature is increased.

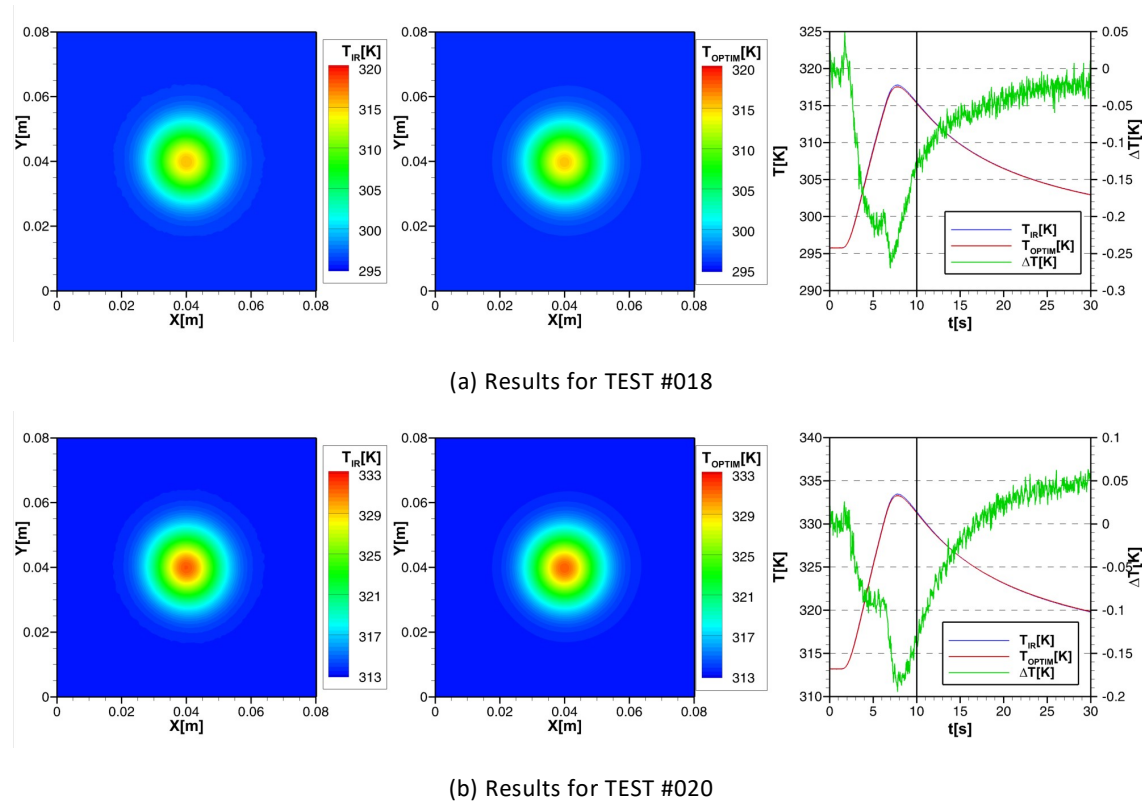
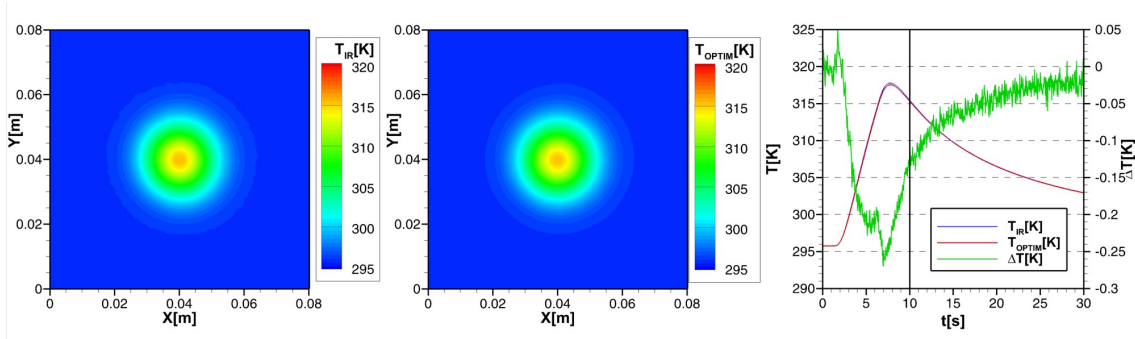
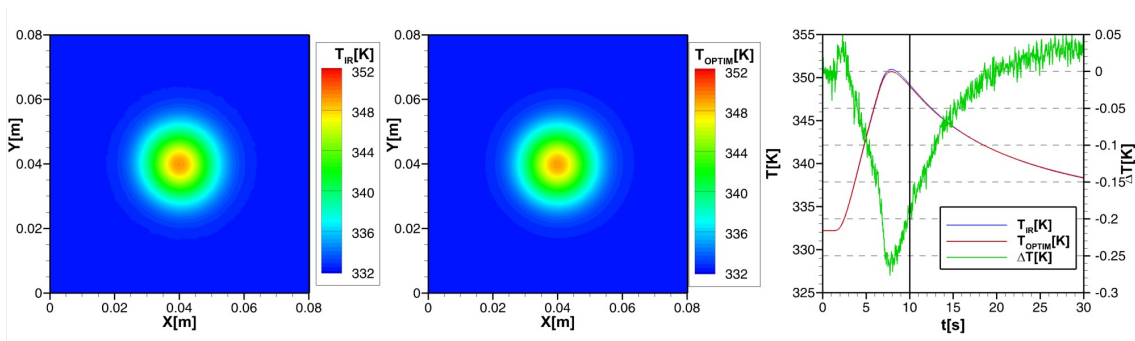


Figure 21 - Results comparison for the optimisation run #6 on the temperature range [22 – 40 °C]

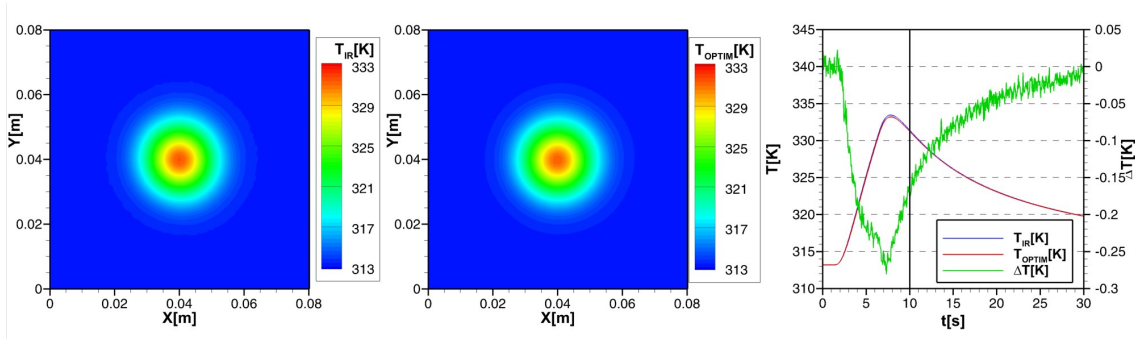


(a) Results for TEST #018

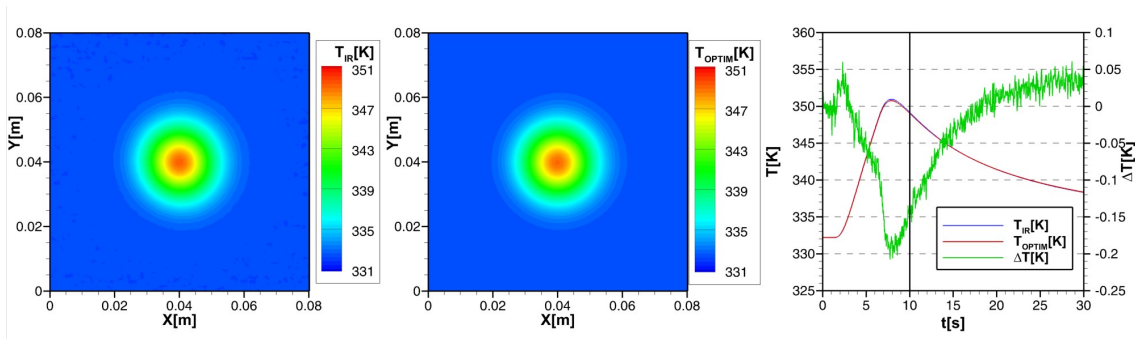


(b) Results for TEST #024

Figure 22 - Results comparison for the optimisation run #7 on the temperature range [22 – 60 °C]

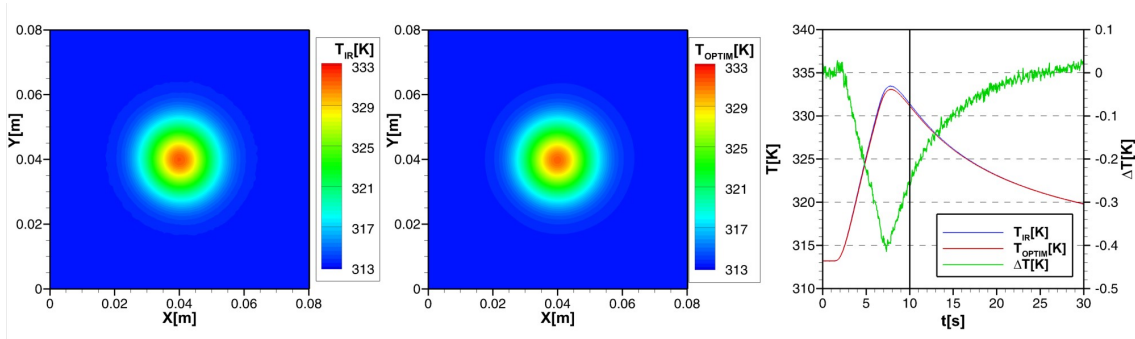


(a) Results for TEST #020

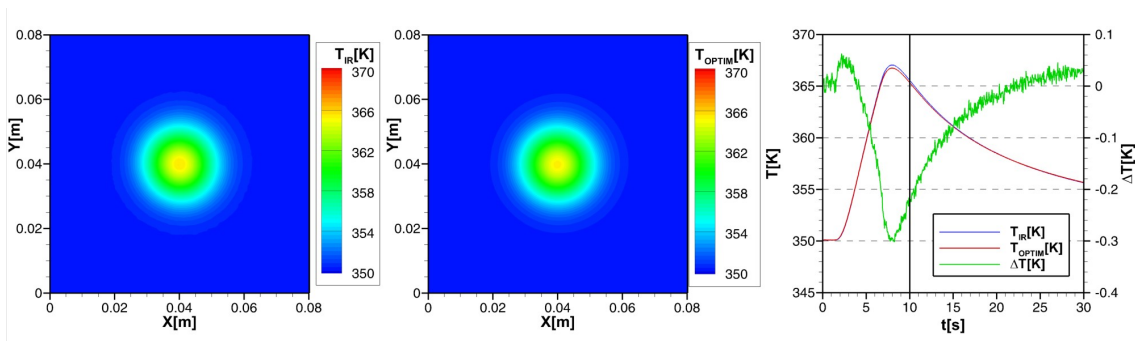


(b) Results for TEST #024

Figure 23 - Results comparison for the optimisation run #8 on the temperature range [40 – 60 °C]

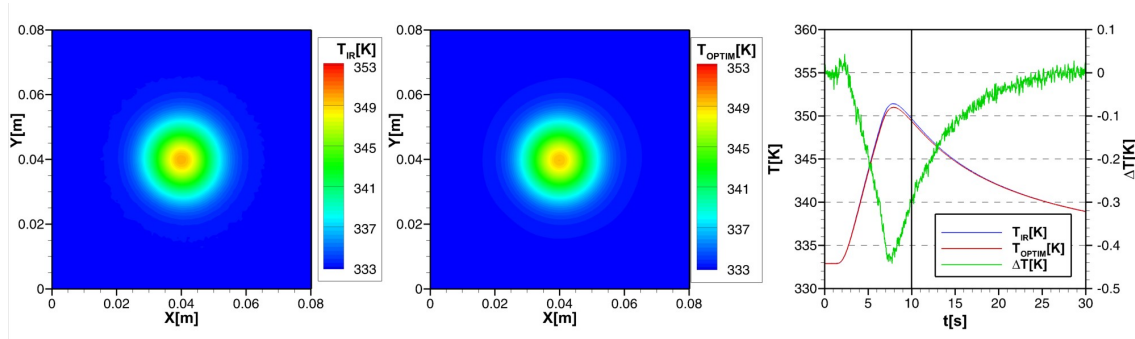


(a) Results for TEST #020

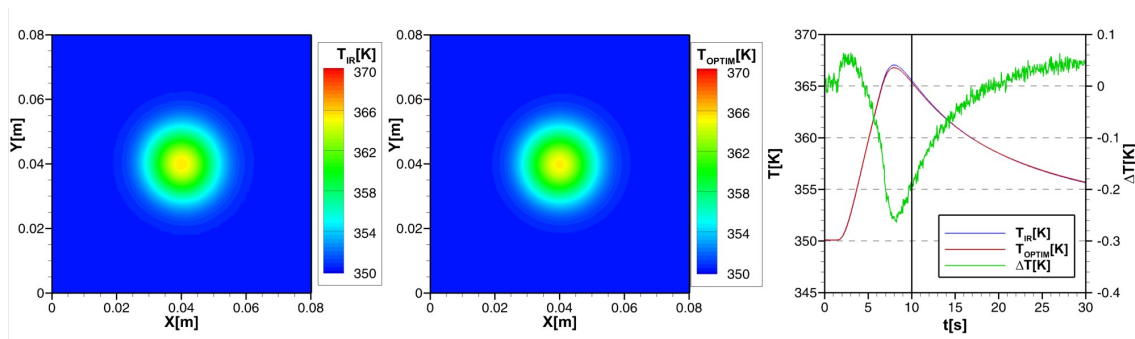


(b) Results for TEST #027

Figure 24 - Results comparison for the optimisation run #9 on the temperature range [40 – 80 °C]



(a) Results for TEST #024



(b) Results for TEST #027

Figure 25 - Results comparison for the optimisation run #10 on the temperature range [60 – 80 °C]

Figure 26 to Figure 29 shows the thermophysical properties as a function of temperature resulting from each optimisation run. As previously, the 20 °C-increase of temperature during each test is taken into account to extend the applicability of the thermal laws. As a result, each temperature range has a magnitude of 40 °C.

All properties increase as a function of temperature on the range of interest for the quasi-isotropic laminate configuration. But the slope of the different curves seems to increase as temperature increases.

According to the composite laminate theory, specific heat and thermal conductivity in the through-thickness direction of a quasi-isotropic and a unidirectional laminate must be identical whatever the stacking sequence if a multiple of 4 plies is considered. The values identified for the specific heat (Figure 26) are a bit lower at low temperatures to finally match at high temperatures. Instead, the thermal conductivity k_{zz} (Figure 29) is surprisingly much higher for the quasi-isotropic material especially for the highest temperatures. The material thickness is identical. As a consequence, discrepancies may be related either to differences between the material composition of the 2 panels or to the accuracy of the optimisation methodology.

Reproducibility of the results should be evaluated from measurements performed on coupons extracted from a different panel manufactured by CEiiA.

According to the laminate theory, the in-plane component of the thermal conductivity tensor must be equal in a quasi-isotropic stacking sequence and the associated value must be:

$$k_{xx}^{ISO} = k_{yy}^{ISO} = \frac{1}{2}(k_{xx}^{UD} + k_{yy}^{UD})$$

Instead, the thermal conductivity k_{xx} (Figure 27) is lower than the component k_{yy} (Figure 28). For instance, $k_{xx} = 3.20 \text{ W/m/K}$ while $k_{yy} = 3.36 \text{ W/m/K}$ at 20°C . An interesting feature is that the in-plane average value is equal the value predicted by the laminate theory calculated from the unidirectional laminate results:

$$\frac{1}{2}(k_{xx}^{ISO} + k_{yy}^{ISO}) = \frac{1}{2}(3.20 + 3.36) = 3.28 = \frac{1}{2}(k_{xx}^{UD} + k_{yy}^{UD}) = \frac{1}{2}(5.76 + 0.795)$$

Discrepancies in the in-plane components identification coming from the optimisation method are questionable because it can only depend on geometrical factors. The same square geometry has been used for both characterisations and a perfect alignment of the material on the coupon holder of the BLADE facility is granted before each test. Such discrepancy can be obtained for instance if a rectangle test coupon is modelled by a square geometry.

Another explanation may be related to the manufacturing process of the quasi-isotropic composite laminate. However the manufacturing process of the unidirectional laminate is trivial, a small shift in the angles of the plies can affect the resulting properties significantly. $\pm 45^\circ$ -plies must be aligned perfectly to get a perfect quasi-isotropic composite laminate. A misalignment is also compatible with an agreement of the average in-plane values calculated from the 2 different laminates.

Please note that the manufactured panels were easier to bend in one direction than the other. As a consequence, the accuracy of the stacking sequence was questioned before the tests to begin. **Reproducibility of the results should be evaluated from measurements performed on coupons extracted from a different panel manufactured by CEiiA.**

Compared to the unidirectional laminate, since both in-plane components of the thermal conductivity tensor are similar in a quasi-isotropic stacking sequence, the sensibility of the optimisation method is identical in both in-plane directions x and y . As a consequence, the identified values presented in Figure 28 for k_{yy} are more continuous than the values presented for the other material configuration in Figure 14.

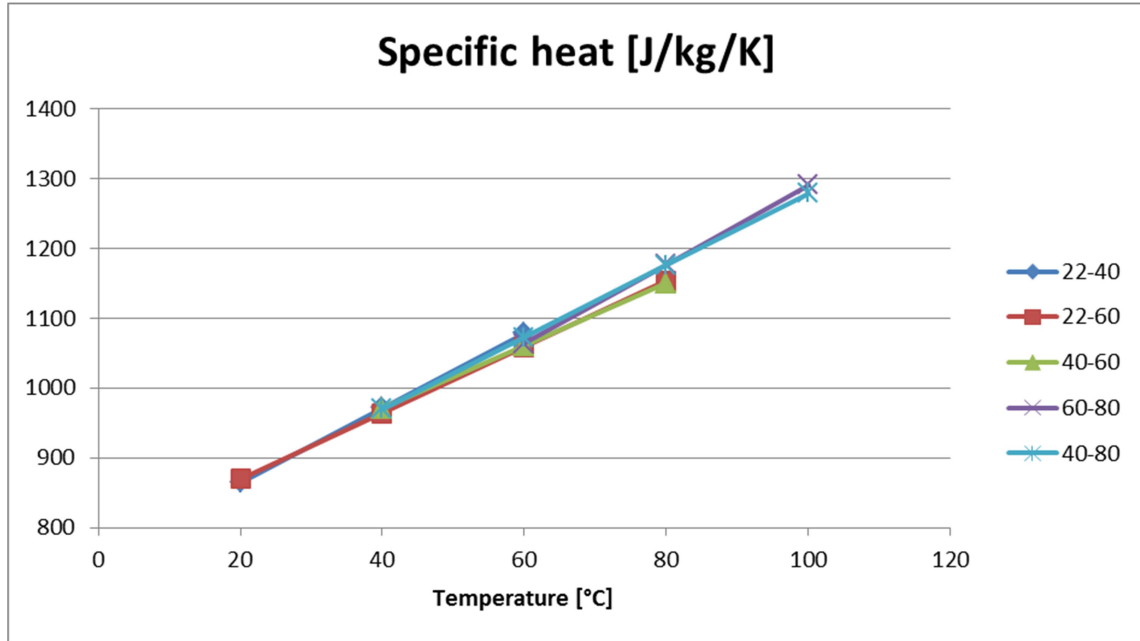


Figure 26 - Comparison of the specific heat identifications on the different temperature ranges for the T700GC-M21-QI8 composite laminate

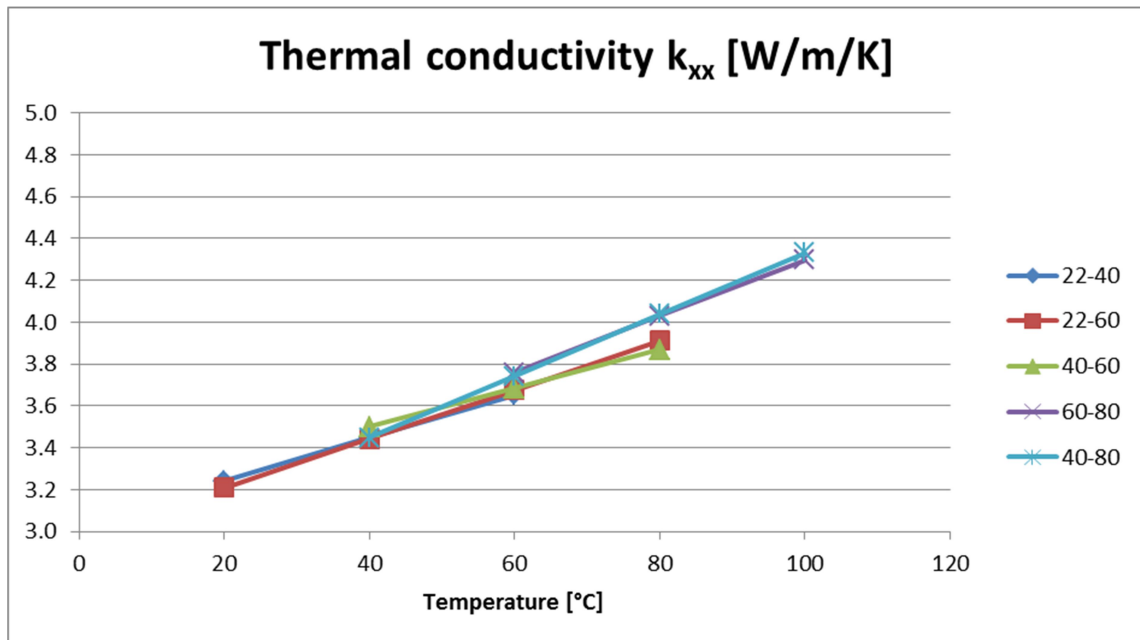


Figure 27 - Comparison of the thermal conductivity k_{xx} identifications on the different temperature ranges for the T700GC-M21-QI8 composite laminate

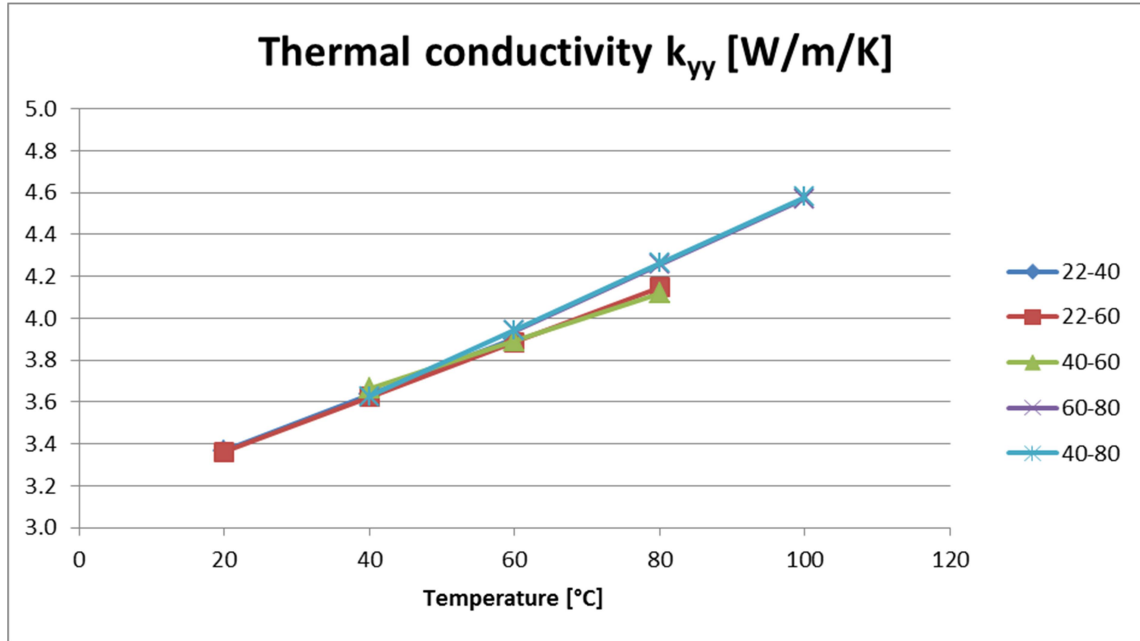


Figure 28 - Comparison of the thermal conductivity k_{yy} identifications on the different temperature ranges for the T700GC-M21-QI8 composite laminate

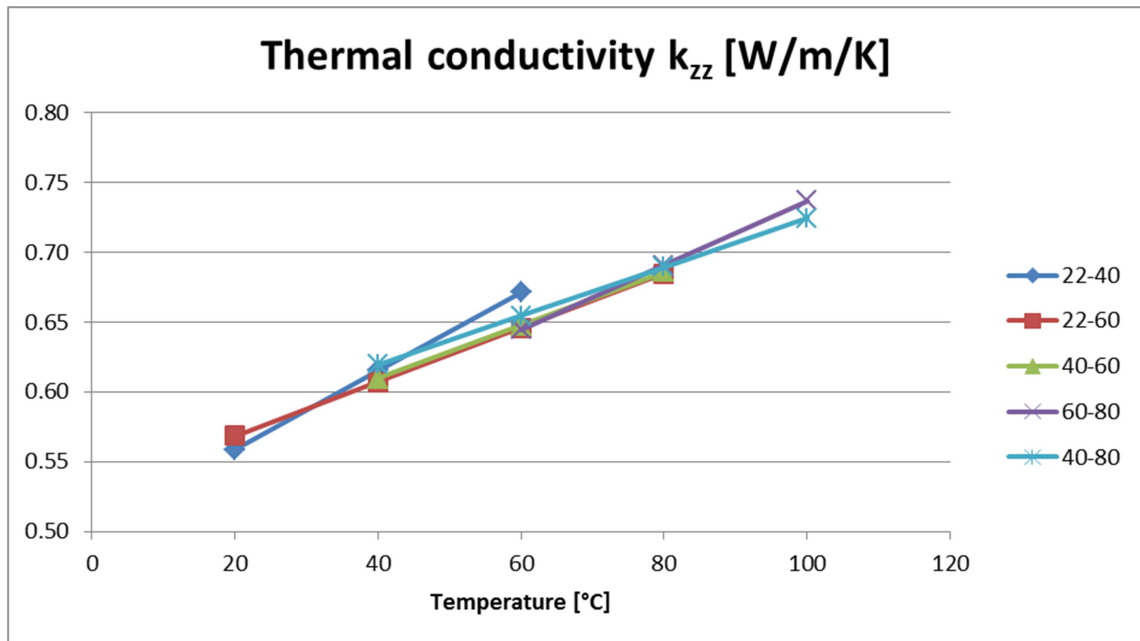


Figure 29 - Comparison of the thermal conductivity k_{zz} identifications on the different temperature ranges for the T700GC-M21-QI8 composite laminate

The thermal behaviour of the laminate is not linear as a function of temperature and higher order polynomial laws may be considered to assess a relevant temperature-dependency of the thermophysical properties. Figure 30 to Figure 33 show a post-processing identification of the thermal laws on the whole temperature range from the previous piece-wise linear results. A second order polynomial law (in the plain black line) is compared to a first order linear law (in the plain red line). Both are fitted from the previous results plotted in blue symbols.

Considering the uncertainties and relative error obtained with the optimisation process from the IR measurements, the first order linear behaviour provides a satisfactory and relevant representation of the evolution of the properties on the temperature range of interest.

Same conclusions than previously can be drawn. The use of higher order polynomial laws should be done carefully because extrapolation beyond the temperature range used for the identification may result in non-physical results. **Additional results are required at higher temperatures to assess more accurate information about the temperature evolution of the thermophysical properties and avoid hazardous extrapolations.**

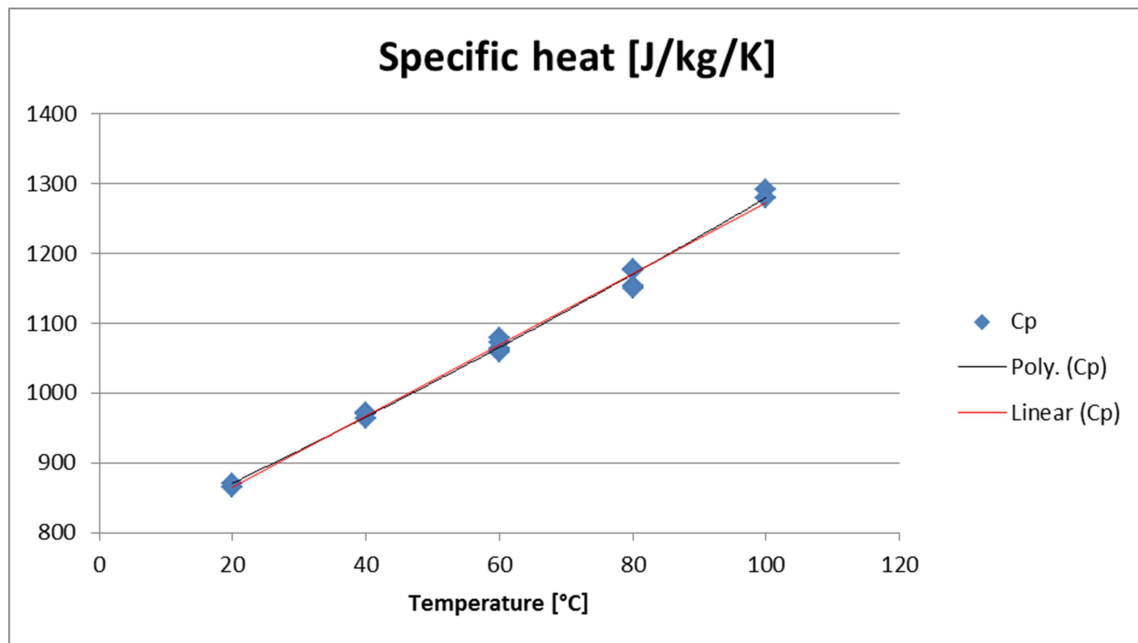


Figure 30 - Identification of the specific heat on the whole temperature range for the T700GC-M21-Q18 composite laminate

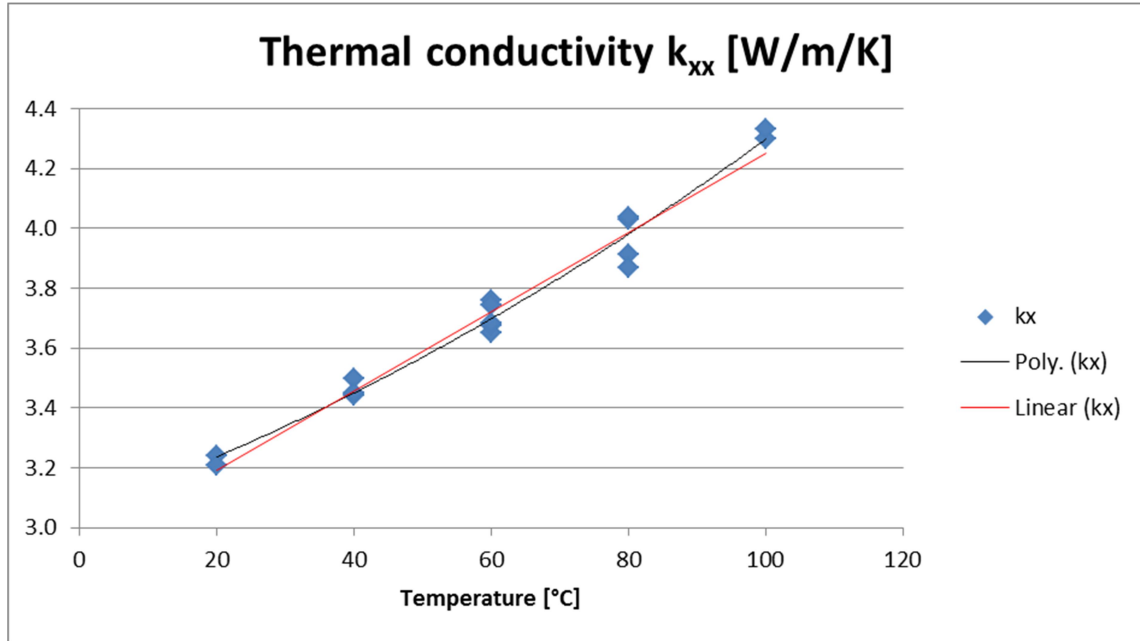


Figure 31 - Identification of the thermal conductivity k_{xx} on the whole temperature range for the T700GC-M21-QI8 composite laminate

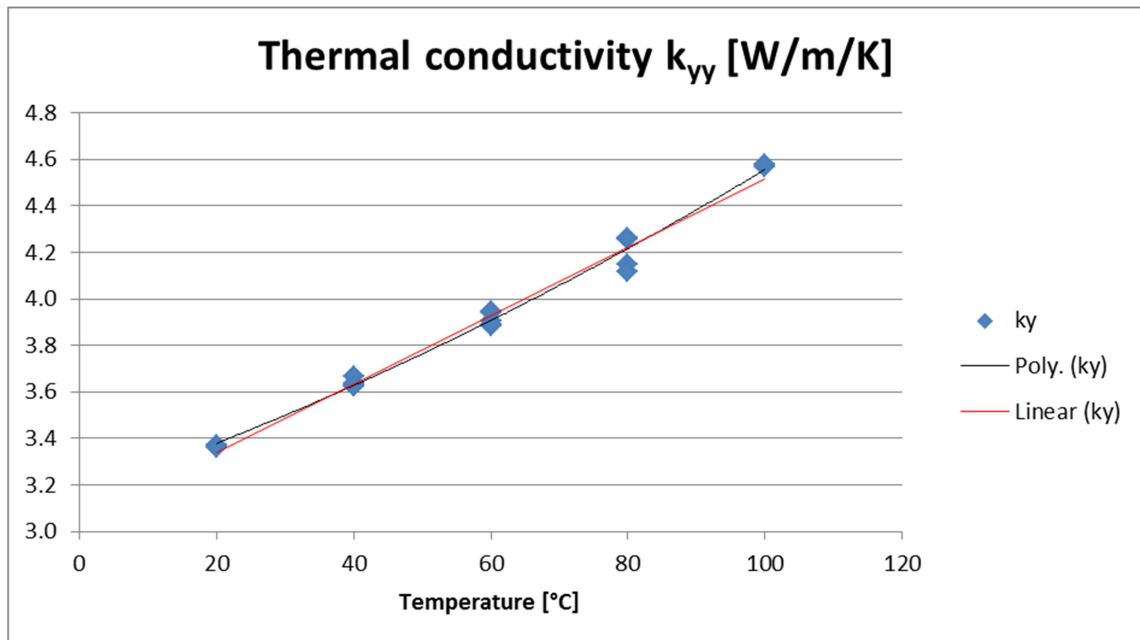


Figure 32 - Identification of the thermal conductivity k_{yy} on the whole temperature range for the T700GC-M21-QI8 composite laminate

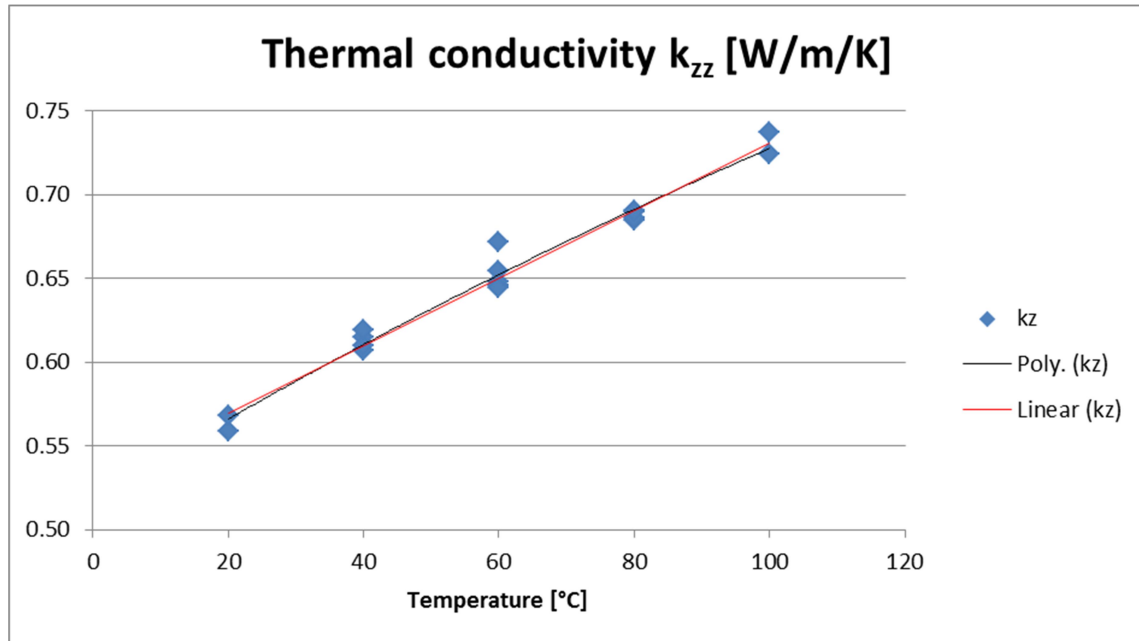


Figure 33 - Identification of the thermal conductivity k_{zz} on the whole temperature range for the T700GC-M21-QI8 composite laminate

4 THERMOCHEMICAL PROPERTIES

In this section, only preliminary results are presented from the first batch of experiments. Results and analysis will be completed in the second batch of experiments and will be presented in deliverable FSS_P7_ONERA_D7.7.

4.1. Thermogravimetric analysis

Thermogravimetric analyses are performed on different T700/M21 samples thanks to a Setaram Setsys analyzer. The samples weight between 50 mg and 100 mg and their dimensions are 10 x 3 x 2 mm with the fibres along the longest direction. The samples have been extracted from unidirectional plates (8 plies thick). Experiments are performed under different atmospheres: air and nitrogen (without oxygen) and with numerous heating rates: 2, 10 and 20 degrees per minute. The objectives of these experiments are to characterize the principal chemical reactions that lead to a thermal degradation of the composite material induced by the environment condition (temperature and gas) and monitored here by the mass loss.

4.1.1. Neutral atmosphere: Nitrogen ambience

The mass loss measured under nitrogen atmosphere is consistent with the results from one of our previous studies on T700GC/M21 [5]. The mass loss is between 20% and 25% for each sample and for all temperature ramps. The only difference is that degradation begins at a lower temperature (around 580K) for a ramp of $2K / min$ versus 600K for 10 and $20K / min$. Mass loss versus temperature is presented in Figure 34. The evolution of this mass loss could be split in three main parts. In a first part, the mass loss rate is very limited (only few percent of mass loss) before a high increase of the mass loss rate at around 600 K. This high increase of mass loss from 0.1 to 23 % appears in short range of temperature (between 580 K and 700 K) whatever the ramp of temperature. However, a shift of the onset of this decrease is observed for the lowest temperature ramp (as mentioned earlier) and corresponds to the second step of the thermal degradation of the composite material. After, 700 K the mass loss rate seems constant to around $0.01 \% / K$ and corresponds to the last step.

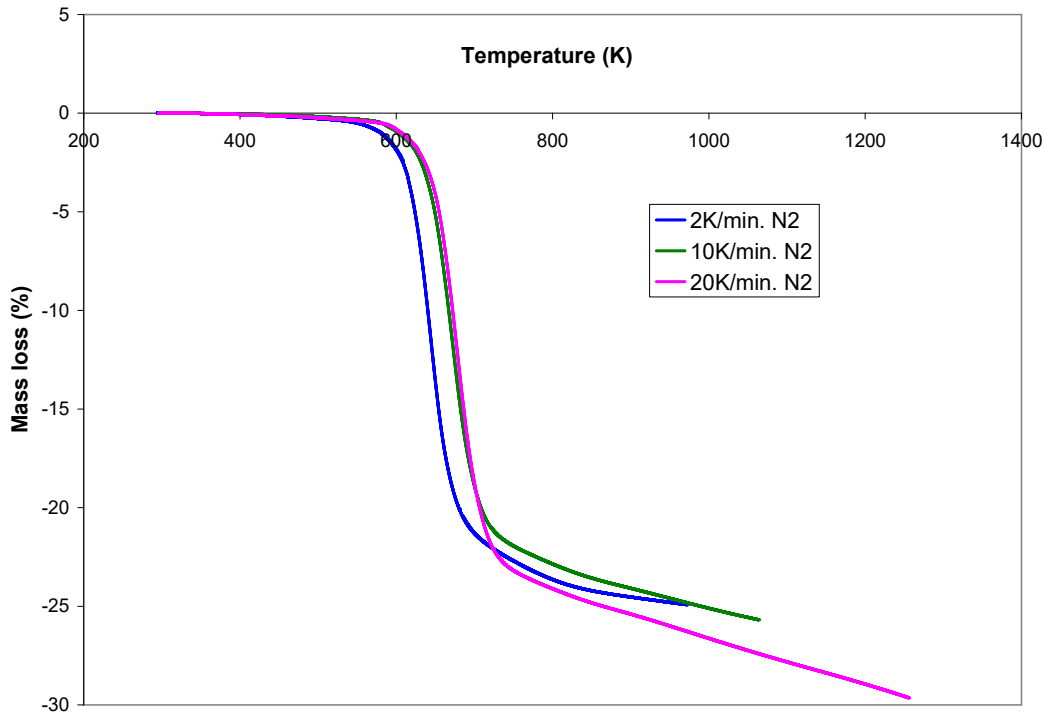


Figure 34 - Mass loss with temperature under nitrogen atmosphere at different ramp temperatures

4.1.2. Oxidation atmosphere: Air ambience

Figure 35 presents the mass loss as a function of temperature for different temperature ramps under air. The first comment is the influence of the oxygen on this evolution with respect to the mass loss measured under nitrogen atmosphere (Figure 34).

For the temperature ramp of $2\text{ K} / \text{min}$, the mass loss evolution exhibits 3 different reactions. The two first ones represent the transformation of the epoxy resin in char in a first step and its oxidative degradation in a second step. For temperatures above 850 K , the last reaction is the oxidation of carbon fibres.

For the temperature ramp of $10\text{ K} / \text{min}$, it is more difficult to distinguish the three reactions we observed in the previous case. A first reaction occurs above 600 K and the degradation seems continuous between 750 K and 1200 K . Oxidation of the sample is not complete and the final mass loss is around 80 %.

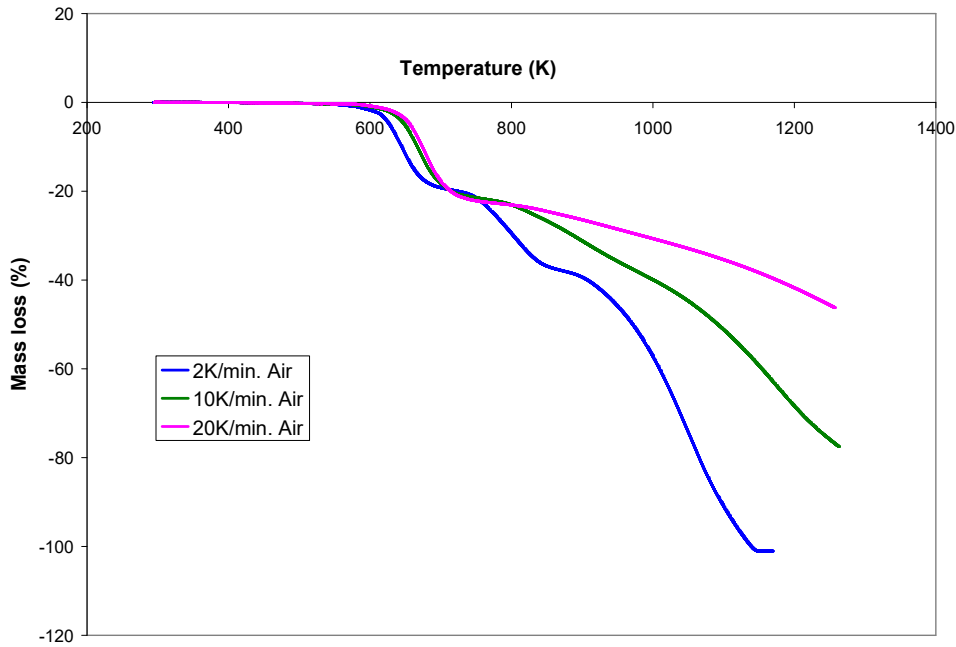


Figure 35 - Mass loss with temperature under air at different ramp temperatures

For the highest temperature ramp of 20 K/min , the mass loss is similar to the experiments realised without oxygen for the same temperature ramp, only the degradation above 850 K differs. The total mass loss is 40% which roughly represents the mass fraction of epoxy resin in the composite (Figure 36).

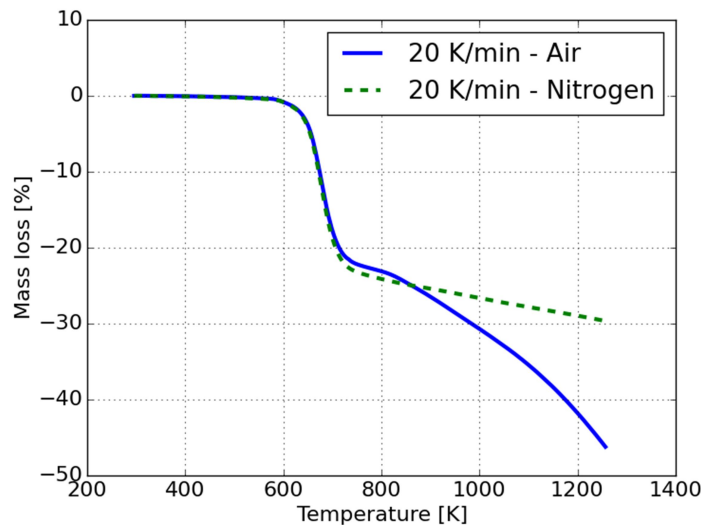


Figure 36 - Mass loss with temperature under air at different ramp temperatures

The various observed reactions exhibit a competition between oxidation reactions, as observed for 2 K/min on Figure 34 and pyrolysis reactions as presented in Figure 35 . Oxidation is a surface

phenomenon that needs a sufficient amount of oxygen to occur correctly. In the case of a temperature ramp of 2 K/min , there is enough time to oxidise completely the studied sample. For 10 K/min , we assume that the sample is thin enough and the temperature ramp low enough to ensure a correct thermal equilibrium. In this case, oxidation begins on the surface of the sample and progressively degrades it. But the kinetic of the oxidation reaction is quite slow and also depends on the diffusion of oxygen near the surface. After only 2000 s , the temperature of the sample reaches 600 K that corresponds to the pyrolysis temperature of the epoxy matrix. From this time, a competition between oxidation on the surface and pyrolysis in the centre of the sample takes place. This is particularly relevant for the ramp of 20 K/min in which the degradation profile under air is very similar to the results obtained under nitrogen. That implies a highly dominant pyrolysis reaction on the mass loss with respect to the oxidation one.

Figure 37 presents the mass loss of the composite samples versus time for the different temperature ramps to underline the kinetics of the oxidation reactions. These time evolutions emphasize the last remarks concerning the oxygen diffusion within the material. At low temperature ramp, the three reactions are clearly monitored by the mass loss evolution. On the opposite, the char oxidation reaction is less observable on the mass loss evolution for 10 and 20 K/min temperature ramps than for the 2 K/min one.

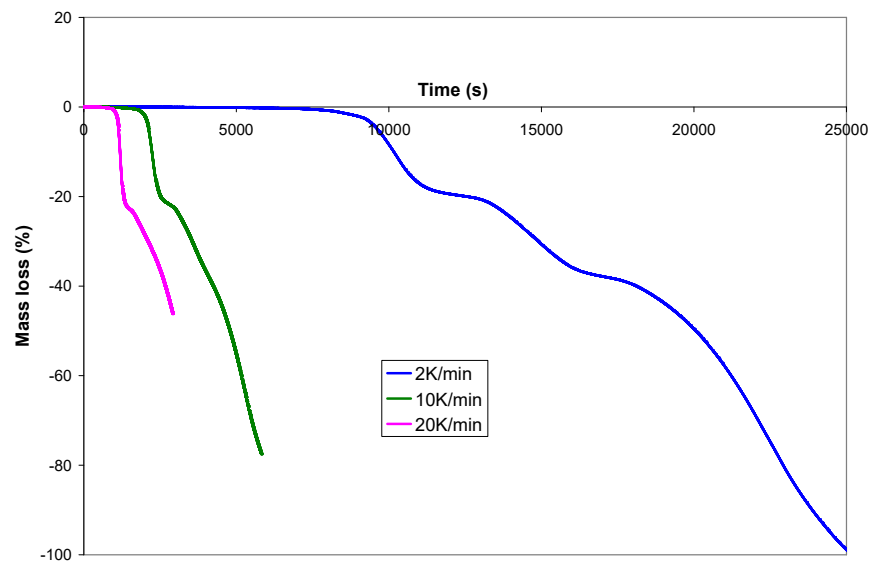
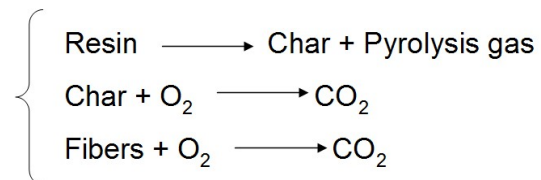


Figure 37 - Mass loss versus time under air at different ramp temperatures

4.2. Discussion and further works

The decomposition under nitrogen presents only one global reaction which is interpreted as a reaction of pyrolysis due to the lack of oxygen in the test atmosphere. The decomposition with air shows 3 successive reactions with no residue in the case a temperature ramp of 2 K / min . The most obvious interpretation of these 3 reactions of degradation consists in a first step of the pyrolysis of the matrix producing char (similarly to the reaction observed in nitrogen atmosphere) and for the next two reactions, in oxidation reactions of the char and carbon fibres respectively. The kinetics of oxidation degradation of T700 fibres studied by Feih and Mouritz [6] shows an almost complete degradation between 970 and 1250 K whereas the decomposition under inert atmosphere exhibits only 0.8% mass loss.

The second interpretation concerns the pyrolysis reaction under nitrogen (Figure 34) which is seen as the decomposition the epoxy matrix resin M21 in volatile organic compounds and a carbon based solid residue named char. This pyrolysis reaction is also observed with air atmosphere but it seems to be altered by the presence of oxygen. The studies of Rose *et al.* [7] and De Fenzo *et al.* [8] on the decomposition of epoxy resins under oxidative atmosphere (especially on RTM6 resin which has a very close composition to M21) also observe a modification of the kinetics of the reaction of pyrolysis under air versus inert atmosphere. Rose *et al.* suggest a degradation scheme of the epoxy resin where a pre-oxidation of the material (with little emission could delay the pyrolysis in oxidative atmosphere). Then the char residue is degraded by oxidation and only provides volatile compounds, which correspond to the second reaction of decomposition of the experiment under air with a ramp temperature of 2 K / min . Thus the degradation model of T700GC/M21 can be resumed by the three following reactions:



Kinetics of the pyrolysis reaction can be described by an Arrhenius law following a reaction rate α_p . The equation is modified in order to exhibit the temperature ramp β [5]:

$$\frac{\partial \alpha_p}{\partial T} = \frac{1}{\beta} (1 - \alpha_p)^{n_p} A_p \exp\left(\frac{-EA_p}{r_g T}\right)$$

The parameters of the Arrhenius law can be determined thanks to the TGA experiments. For the pyrolysis reaction, it is possible either to keep the same Arrhenius parameters for nitrogen and air atmosphere either to look for another optimal set of parameters under air. These two possibilities have been investigated and having two different sets of parameters leads to the best description of our experimental results. The simulation of reactions kinetics thanks to TGA results can only be performed under the assumption of an ideally thermally thin material. This condition ensures a thermal equilibrium and a good diffusion of oxygen around the sample.

Project: Mitigating risks of fire, smoke and fumes
Reference ID: FSS_P7_ONERA_D7.4
Classification: Public



Due to the lack of confidence on the data concerning the oxidation reaction, the identification of the parameters is not done yet and will be presented in the next deliverable. These experiments underline the necessity to establish standard approach concerning the characterisation of the thermo-degradation of composite materials.

For the next deliverable, this thermo-chemical characterisation will be complemented with DSC experiments and with analysis of gas emitted during the TGA experiments.

5 THERMO-MECHANICAL PROPERTIES

Concerning the mechanical and thermo-mechanical material properties, the decomposed (by fire) composite materials have not often been studied and clearly not considering the full spectrum of already existing thermo-mechanical, time and temperature dependent, material models. The objective is to complete mechanical tests on a standard CFRP composite material to confront and sum up the different test results to reach a better physical understanding of the composite material behavior above ambient temperatures, hence improving knowledge to give a more physical and universal foundation to composite material models. The main ideas are for instance to complete existing material tests results with (1) compression tests along the fibers direction at high temperatures, (2) tests at various (but still low) velocities, and (3) tests at temperatures above the glassy transition and/or for charred material states.

In the following sections, only preliminary results are presented from the first batch of experiments. Results and analysis will be completed in the second batch of experiments and will be presented in deliverable FSS_P7_ONERA_D7.7.

5.1. In-plane compression

The purpose of this experimental study is to characterize the evolution of carbon/epoxy material compressive behaviour with respect to the increase of the temperature. At room temperature, two normative procedures coexist for the characterization of the compressive mechanical properties in the fiber direction: ASTM D3410 and ASTM D695. The main difference between the two normative procedures is the way of applying the load to the specimen. In the ASTM D3410, a shear loading is applied to the specimen through the tabs whereas a compressive end loading is applied to the specimen in the ASTM D 695. Finally, mixed solution can be used in which the loading is applied to the specimen by shear and end loadings. For the present study, two experimental setups were assessed. The first one allows applying shear loading as proposed in the ASTM D3410. And the second one can be used to apply a mix loading with shear and end loadings. The two experimental setups were compared to choose the more accurate one. To be able to perform such a comparison, the specimen geometry has to be validated regarding the specificity of this study. High temperature tests have to be performed on the specimen. Consequently the tabs should be able to carry the load at temperatures close to 200°C. Classically glass/epoxy composite materials with a T_g lower than 200°C are used to manufacture specimens tabs. Such tabs are not suitable and two alternative solutions have been studied: perform the test without tabs or with aluminum tabs. The tests have been performed at room temperature with the ASTM D3410 experimental setup for three different specimens: the first one without tabs, the second one with aluminum tabs and the last one with classical glass/epoxy composite material tabs. A total of 30 tests have been performed to set up and assess the different test protocols. Results are summarized in Table 10.

The comparison based on the maximum stress value obtained during the test shows that the results obtained with the glass/epoxy tabs and the aluminum tabs are similar whereas the results obtained

without tabs are considerably lower. This leads to the conclusion that to be able to perform tests at high temperatures, aluminum tabs will be used in this study.

Tabs	Maximum stress [MPa]
Glass/epoxy	1095
Aluminum	1053
Without	660

Table 10 - Comparison of the maximum stress obtained with glass/epoxy tabs, aluminum tabs and without tabs

Note that the specimens cutting technique (from the composite plates with the glued aluminum bands) had to be sub-contracted (the ONERA usual diamond-disk cutting tools being not appropriate). As the process used by the sub-contractor turned out to produce delamination at the edges of the specimens, part of the composite plates provided by CEiiA had to be used to solve this problem. So ONERA has manufactured two new composite plates for the coming test campaign (second batch test specimens and results).

The comparison of the results obtained with the two available experimental setups is plotted in Figure 38.

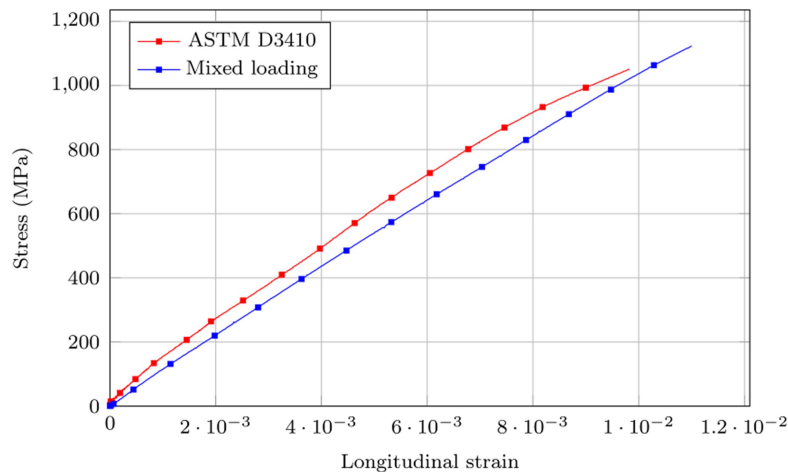


Figure 38 – Stress-strain curves obtained for compressive tests on T700GC/M21 [0]₁₆ laminates with two different experimental setups: ASTM D3410 (in red) and ONERA mixed loading (in blue)

In Figure 38, the stress-strain curves are plotted for the two experimental setups. The results obtained with the ONERA mixed loading setup exhibit a linear behavior until fragile failure, whereas for the ASTM D3410 setup the behavior appears to be more non-linear with a higher apparent modulus. Finally, the maximum stress is slightly higher with the ONERA mixed loading setup than with the ASTM D3410 setup. For both setups, the maximum compressive stress is lower than the one claimed by the manufacturer (1300 MPa). Consequently, the ONERA mixed loading setup gives a maximum stress value closer to the manufacturer one. According to these results, the ONERA mixed loading setup has been chosen to perform the tests at high temperatures.

To fully validate the experimental protocol proposed in this definition part for the study of the longitudinal compressive behavior, tests with gauges glued on both sides of the specimens had to be performed in order to assess that the specimens were not undergoing buckling. The stress strain curves obtained from the 2 strain gauges on a given specimen are plotted in Figure 39. Both curves superimposed until the final failure of the specimen which confirms the absence of buckling during the test.

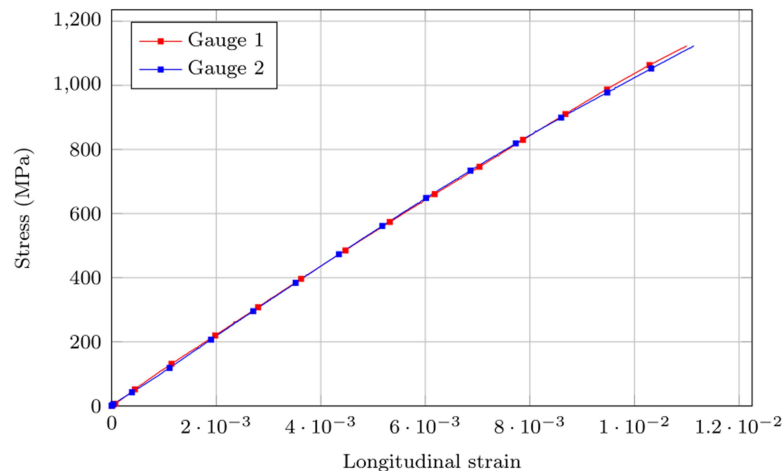


Figure 39 – Stress-strain curves obtained for compressive tests on T700GC/M21 [0]₁₆ laminates with gauges glued on both sides of the specimen.

Concerning the transverse compressive tests campaign, the same study has been performed leading to the same conclusions. Consequently, the protocol to perform the experimental characterization of the in-plane compressive properties under high temperature of the T700GC/M21 has been fully validated in this preliminary study and the full set of experimental results will be presented in the deliverable containing the second batch of experimental results.

5.2. Dynamic Mechanical Analysis

5.2.1. DMA experiments on unidirectional laminate

Dynamic Mechanical Analysis (DMA) is performed in this study in order to investigate mechanical properties of T700GC/M21 with temperature. Dynamic mechanical properties refer to the response of a material as it is subjected to a periodic force. These properties may be expressed in terms of a dynamic modulus, a dynamic loss modulus, and a mechanical damping term. DMA is conventionally used to study and characterise materials. It is most useful for studying the viscoelastic behaviour of polymers. In this study, DMA is used to characterise mechanical and physical properties of a material with temperature.

DMA experiments are performed on a Metravib DMA+1000. Samples are 2 mm-thick, around 10 mm-wide and the working length is about 30 mm. Tensile tests are performed with an imposed periodic displacement of $2 \cdot 10^{-6}$ m with a frequency of 1 Hz and with a temperature range from 300 K to 600 K (20°C to 350°C). For this last temperature, the sample is far above its glass transition temperature (T_g) and characterisation becomes more difficult. Two different laminates were studied: unidirectional 0° (UD0) or unidirectional 90° (UD90). The Figure 40 presents the evolution of the loss factor as function the temperature applied in the test chamber.

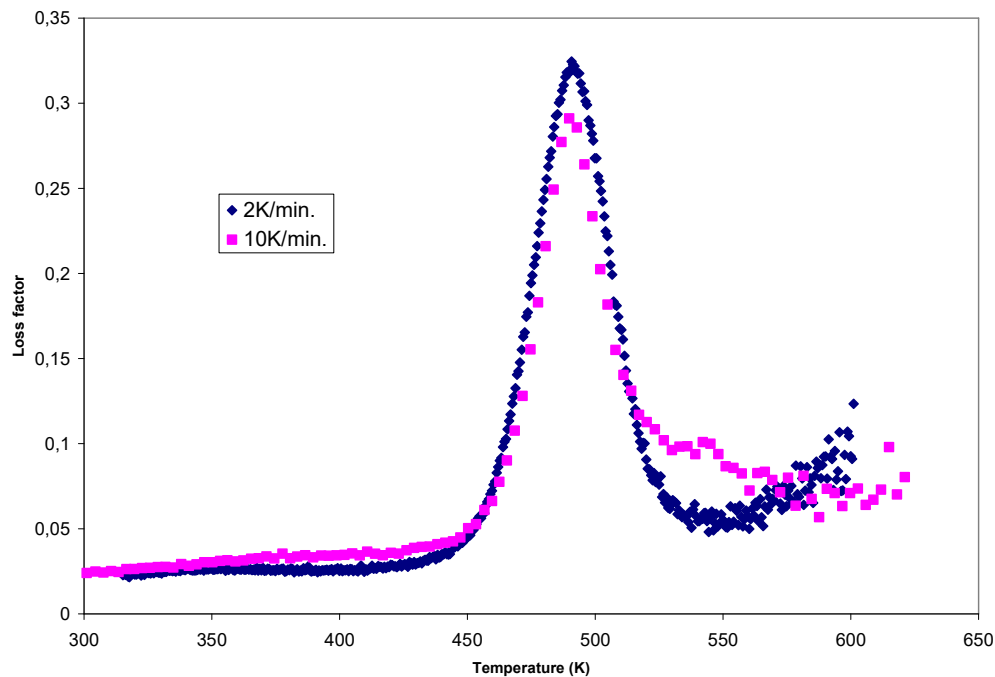


Figure 40 -DMA on an UD90 sample, loss factor with temperature

The maximum of the loss factor is reached for 490 K and can be assimilated to T_g . Failure occurs for the sample heated at 2 K / min at a temperature of around 550 K and several matrix cracks are also visible.

Due to the limitation of the device, the experiments are stopped at 600 K. Indeed, the DMA device is unable to measure any dynamic tensile modulus and induces an ending of the experiment. The main hypothesis is due to the degradation of the matrix by pyrolysis (accorded to our TGA results presented previously in section §4.1.2) which results in such a decrease of the sample stiffness.

This hypothesis is confirmed by the evolution of the apparent Young modulus as function of the temperature presented in Figure 41 of an UD90 laminate between room temperature and about 600 K.

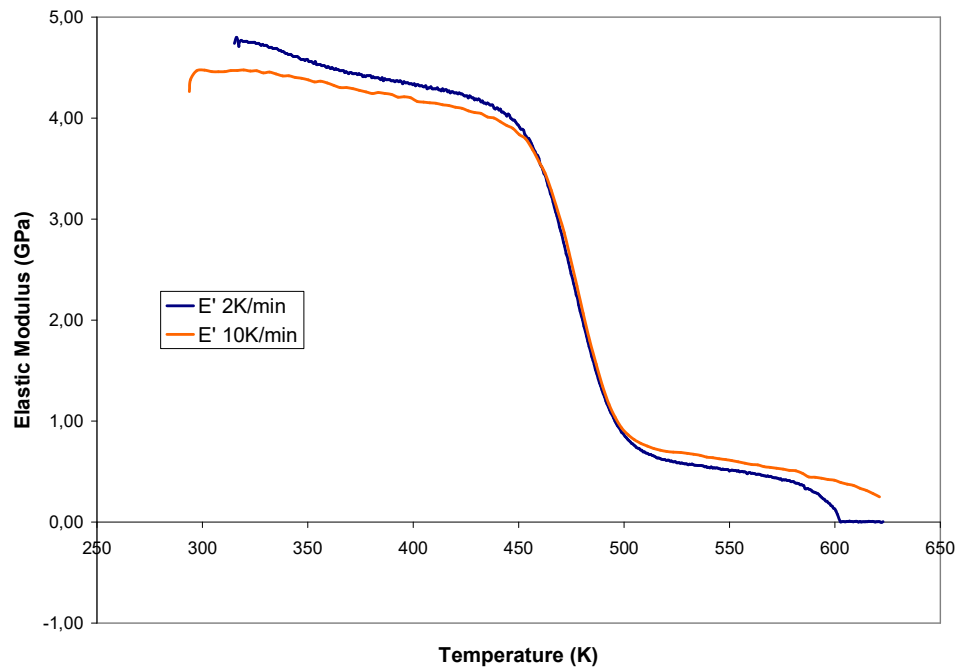


Figure 41 -DMA on an UD90 sample, elastic modulus (GPa) with temperature

Experiments are performed with temperature ramps of 2 K / min and 10 K / min as mentioned before. Results are very similar in both cases. There is a slight decrease of the elastic modulus with temperature below the glass transition temperature (T_g). At T_g , the modulus drops from around 4 GPa to 500 MPa.

The complex modulus is around 5 GPa at room temperature whereas the Young modulus obtained for this laminate with static tests is around 8–9 GPa [9]. The complex and Young modulus have the same order of magnitude but the DMA experiment conditions (frequency, amplitude, etc.) still need to be further investigated to properly compare both values and conclude on the efficient of characterisation of the transverse modulus by DMA.

Note that some attempts of experiments were also performed on UD0 samples, the results of which are not discussed in the present report.

5.2.2. Results and further works

Dynamic Mechanical Analysis seems clearly interesting for making a link between thermos-degradation of the composite material (assessed by ATG or DSC) and the mechanical behaviour as function of the temperature. Nevertheless, it is clear that the main parameter remains the T_g for the decrease of the mechanical properties and an important work is required for distinguishing the influence of the mechanical properties due to the temperature (mainly due to the evolution of the chain mobility as function of the temperature) from the thermal degradation of the composite (pyrolysis of the matrix, char and fibres oxidations...). Nevertheless, to succeed in, it is important to propose standard procedures in order to characterise such influence. The obtained results clearly needs to be confirmed by an improvement of the experimental conditions in order to load not only the resin but also all the composite behaviour. Experimental conditions such as the frequency, amplitude and the type of loading (applied displacement or load) need to be investigated.

6 CONCLUSIONS AND RECOMMENDATIONS

6.1. Conclusions

The BLADE facility, developed by ONERA, has been used to carry out thermal characterisations of the T700GC/M21 selected composite laminate. Specific heat and thermal conductivity have been assessed as a function of temperature for the virgin state. The orthotropic properties identified from thermographic measurements have shown a significant temperature dependency. A first order polynomial thermal law was accurate enough to capture the transient thermal behaviour of the test coupons subjected to the laser heating within the temperature range of interest. Effects of the stacking sequence have been obviously noticed between the unidirectional and the quasi-isotropic ply layouts. Then, from thermochemical properties assessment, new test coupons will be prepared and conditioned to characterise the properties for the charred state from room temperature.

The characterisation of the thermal degradation of composite laminates needs to propose standard approach. The results concerning the influence of the temperature ramp on the oxidation demonstrated the requirement of such procedures. The TGA results need additional analysis to ensure a pertinent identification of the material thermal degradation model and suitable to fire loading design of composite structures.

Concerning the mechanical and thermo-mechanical material properties, a dedicated test protocol has been selected and assessed to perform compression tests on T700GC/M21 CFRP material above its transition temperature, for different loading speeds. At the end of the FSS P7 T7.1.2 experimental campaign (Primary structure materials - second batch of test results), material tensile, compressive and shear test data will then be available for various temperatures (from ambient to above transition temperature) and test speeds for T700GC/M21 virgin material. These test results will be used in T7.1.3 by WP7.1 partners to assess state-of-the-art models and simulation tools according to this comprehensive set of experimental data.

As for thermal degradation of the material, the characterisation of the influence of this damage evolution on the mechanical properties needs additional developments mainly dedicated to the experimental conditions. The first results presented in this deliverable are encouraging to propose models describing the influence of the temperature on the mechanical properties thanks to DMA device. Nevertheless, it is not clear that the evolution of the mechanical properties measured corresponds to the behaviour of the composite material but more to the evolution of the resin. Further works and development are mandatory.

6.2. Recommendations

The BLADE facility can assess confidently thermophysical properties up to $T = 100\text{ }^{\circ}\text{C}$. Complementary measurements must be conducted to address the material thermal behaviour at higher temperatures.

However, it requires significant technical improvements of the facility. Comparisons with more conventional methods can also be performed to validate the results within the common temperature range and to explore the properties at higher temperatures. Nevertheless, on key feature of the BLADE is the use of 2D temperature measurements and 3D simulations based on a direct orthotropic heat conduction solver to assess the properties simultaneously. As a consequence, all properties are coherent with each other while the conventional combination of flash method (semi-infinite medium), DSC and density measurements can result in biased thermal conductivity estimations. Moreover, additional tests must be conducted on coupons extracted from different panel to confirm the conclusion about results reproducibility.

The TGA and DMA experimental protocols need to be improved in order to be representative of the physical properties of the material during fire loading. This first results underline the necessity to make compromise between the complexity of the physics involved in the evolution of the apparent properties (chain mobility, chemical reactions...) and the model to propose for fire design (simplified approach, phenomenological thermal and mechanical behaviour).

7 REFERENCES

- [1] M. Oliveira et al., Future Sky Safety, Plan of Experiments - Primary Structures Materials - Final Requirements, Selection and Specification of Materials and Tests, D7.1, September 2015.
- [2] E. Deletombe et al., Future Sky Safety, Project Plan P7 - Mitigating the risk of fire, smoke and fumes (V3.0), D8.1 - Appendix P7, September 2015.
- [3] P. Reulet and G. Leplat. An inverse method for experimental determination of temperature dependent thermal conductivities and specific heat of orthotropic materials. In *ITCC 2011 - International Thermal Conductivity Conference*, Chicoutimi, Quebec, CANADA, 2011.
- [4] G. Leplat and V. Biasi. Experimental and numerical thermal response analysis of laser-induced composite decomposition. In *FRPM 2015 - 15th Fire Retardancy and Protection of Materials meeting*, Berlin, Germany, 2015.
- [5] P. Beauchene, V. Biasi, C. Huchette, G. Leplat, G. Roger, PRF MADMAX : Caractérisation expérimentale des propriétés physiques du T700M21, *Internal Onera Report (in french) RT 2/21100 DMAE/DMSC*, 2016
- [6] S. Feih, A. P. Mouritz, Tensile properties of carbon fibres and carbon fibre–polymer composites in fire. *Composites Part A: Applied Science and Manufacturing*. 43, 765–772, 2012
- [7] N. Rose, M. Le Bras, S. Bourbigot, R. Delobel, B. Costes, Fire Retardant Polymers Comprehensive study of the oxidative degradation of an epoxy resin using the degradation front model. *Polymer Degradation and Stability*. 54, 355–360, 1996
- [8] A. De Fenzo, C. Formicola, V. Antonucci, M. Zarrelli, M. Giordano, Effects of zinc-based flame retardants on the degradation behaviour of an aerospace epoxy matrix. *Polymer Degradation and Stability*. 94, 1354–1363, 2009
- [9] C. Huchette, Sur la complémentarité des approches expérimentales et numériques pour la modélisation des mécanismes d'endommagement des composites stratifiés *thesis, Université Paris 6*, 2005.